# THE MAGNETIC FIELD OF AB DORADÛS

**Graham Richard Pointer**

**A Thesis Submitted for the Degree of PhD**
**at the**
**University of St Andrews**

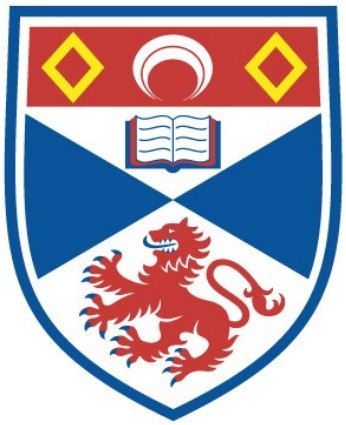

**2001**

THE UNIVERSITY OF ST. ANDREWS

# The Magnetic Field of AB Doradûs

Graham Richard Pointer

Submitted for the degree of Ph.D.

May 2001

# DECLARATION

I, Graham Richard Pointer, hereby declare that this thesis, which is approximately 50000 words in length, has been written by me, that it is the record of work carried out by me and that it has not been submitted in any previous application for a higher degree.

I was admitted as a research student in September 1997 and as a candidate for the degree of Ph.D. in Astronomy in September 1998. The higher study for which this is a record was carried out in the University of St Andrews between September 1997 and May 2001.

In submitting this thesis to the University of St Andrews I understand that I am giving permission for it to be made available for use in accordance with the regulations of the University Library for the time being in force, subject to any copyright vested in the work not being affected thereby. I also understand that the title and abstract will be published, and that a copy of the work may be made and supplied to any *bona fide* library or research worker.

(Graham Pointer)

I hereby certify that the candidate has fulfilled the conditions of the Resolution and Regulations appropriate for the degree of Ph.D. in the University of St Andrews and that the candidate is qualified to submit this thesis in application for that degree.

(Andrew Collier Cameron)

In loving memory of

my grandmother

Greta Kearns

1916-2001

# ACKNOWLEDGEMENTS

Firstly, I would like to thank my parents and my sister for their support and encouragement during this Ph.D.

I would like to thank my supervisor, Andrew Collier Cameron, for his help and advice. I would also like to thank Moira Jardine, Gaitee Hussain and Duncan MacKay for their help with the work on AB Dor's magnetic field.

I would like to thank John Barnes and Tim Lister for their help whenever the computers were annoying me.

Thanks to the members of the Southampton Astronomical Society for encouraging my interest in astronomy.

Thanks to Bryony for all the phone calls, advice and encouragement. And for making me glad I'm not a teacher.

Thanks to Gavin for helping translate the Kippenhahn–Schlüter paper from German.

I would like to thank the Postgraduate Bible Study Group. It was always encouraging, and I looked forward to Thursday evenings. Thanks to Nienke and Helen for the food!

Thanks to Andy, Alastair & Juliet, Graeme, Alastair, Steve, Richard, Bob, Colin, Paul, Alan, Andrew, Michael, Euan & Janet, Alexandra, Mark, Keith & Caroline and Chris for their encouragement and friendship during my time at St Andrews.

Thanks to those I got to know at Leicester– Simon & Hilary, Angela, Dave, Chris & Anne, Chris & Sue, Stu & Kathy, Tim, Julian & Helen– and who have stayed in touch with me over the past few years.

Thanks to Katie for her amusing emails.

Thanks to Eric, Lee, Keith, Miriam and Julian for all the emails.

I would like to thank the Russell Trust Award for paying for me to go observing at La Palma in July 1998, and to use the Isaac Newton Telescope. And to the staff at the Isaac Newton Group for their help there.

I would also like to thank Mike Hill and Simon Harris for allowing me to use the computing facilities at Southampton University to do my corrections. And to Rob Hynes and Luisa Morales for repeatedly lending me the 21 key.

# ABSTRACT

Observations of AB Doradûs, a nearby, rapidly-rotating K0 dwarf are analysed, and the surface magnetic field is shown to be approximated by a potential field.

Evolving the surface magnetic field according to diffusion and the observed differential rotation still yields good correlation between the calculated and observed radial field after 30 days, contradictory to the results of Barnes et al. (1998), leading to the conclusion that there is an additional cause for the evolution of the magnetic field.

The chromospheric magnetic field is modelled as a potential field with a source surface. Using the stability criteria $\mathbf{g}.\mathbf{B} = 0$ and $\mathbf{B}.\nabla(\mathbf{g}.\mathbf{B}) < 0$, places where prominences can be stable are investigated. For agreement with the results of Donati et al. (2000)– that prominences form preferentially near the equatorial plane and at and beyond corotation– it is necessary to add a quasidipolar field of maximum strength $\sim$20G.

# CONTENTS

# LIST OF FIGURES

# LIST OF TABLES

CHAPTER 1

# Introduction

## 1.1 The Sun as a star

Baliunas & Vaughan (1985) and Schrijver (1991) give reasons why studying other stars helps us understand the Sun, and vice versa. These can be summarised as:

1. The effect of parameters such as stellar age, rotation, luminosity and spectral type upon stellar activity can be studied.
2. We can observe the Sun in greater detail than other stars.

## 1.2 Spots

Sunspots have been known for at least two millennia– the catalogue of Wittmann & Xu (1987) lists sunspots dating from as early as 165BC. Priest (1984) reports that the earliest known sunspot was observed by Theophrastus of Athens in 350BC.

Carrington (1858) noticed that in the two years preceding the February 1856 sunspot minimum, the sunspots were confined to within 20° of the equator, but spots forming after minimum tended to be between 20 and 40°.

While observing the Sun in H$\alpha$, (Hale 1908c) noticed vortices connected with sunspots, and suggested that if the solar atmosphere was ionised, then rapid revolution of charged particles should lead to a magnetic field in the spot– where the direction of motion would determine the

polarity of the field in the spot (Hale 1908b; Hale 1908d)– and Zeeman doublets in the spectrum which he predicted were observed (Hale 1908a).

Hale (1908d) investigated the doublets in the spectra of spots, as he wanted to see whether they were circularly polarised. He found that the doublets were circularly polarised in opposite directions, and argued that this indicated that a spot would have a magnetic field. He commented that the doublets would become triplets if observed in a magnetic field at right angles to the lines of force.

Hale et al. (1919) investigated the polarity and strength of the magnetic field in sunspots. If $\gamma$ is the angle between the line of sight and the direction of the magnetic field, and $n_b$ & $n_r$ are respectively the intensities of the blue and red components of a Zeeman triplet then

$$\cos\gamma = \frac{1-\sqrt{\frac{n_b}{n_r}}}{1+\sqrt{\frac{n_b}{n_r}}}.$$

They were able to place sunspots into three categories:

- *unipolar spots* which are small groups of spots with the same polarity,
- *bipolar spots* which are two spots of opposite polarity,
- *multipolar spots* which are groups containing spots of both polarities.

They noted that after the December 1912 sunspot minimum, the polarities of the unipolar spots and leading members of bipolar spots in each hemisphere was opposite to that before the sunspot minimum. One suggested explanation was that the Sun had two active zones– a higher latitude one ($\sim 20-25°$) and a lower latitude one ($\sim 10°$) – and these zones produced spot groups with different polarities. If this were the case, then as the mean latitude of spots drifted equatorward during the sunspot cycle, in each hemisphere the ratio between the numbers of groups with each polarity would evolve, which it failed to do. Nicholson & Sternberg (1934) were able to confirm this polarity reversal two minima later. Further evidence for a ~20–25 year cycle period came from Rush & Trotter (1954), who noted that magnetic storms occured more than twice as frequently before the minima of 1913 and 1933 than they did before the minima of 1923 and 1944.

## 1.3 Magnetic fields on stars

Campbell (1899) observed that the H$\gamma$ line of $o$ Ceti was split into 3 components, with the central component being the strongest. Clerke (1899) suggested that this could be caused by the Zeeman effect, and said that the polarisation of the 3 components would need to be determined before it could be shown whether this was the case. Wright (1910) attempted this but felt his observations were inconclusive.

Hale (1908b) suggested that the Sun could possess a magnetic field. Minnaert (1937) said that it would be difficult to detect a solar–strength magnetic field on another star, but suggested that rapidly rotating stars could have magnetic fields strong enough to be detected by looking for circular polarisation of doublets in the spectrum. Assuming that field strength was directly proportional to the average equatorial velocity (the equatorial velocity is convenient to use, as for the Sun it shows less variation than for other latitudes (Adams 1909)), Babcock (1947) suggested that B, A and early F type stars could have magnetic fields of the order 1.5kG, and he found that some of the absorption lines in the spectrum of 78 Virginis showed circular polarisation which could be explained by the Zeeman effect.

Preston (1971) used the widths of Cr I, Cr II, Fe I and Fe II spectral lines to determine the mean magnetic field strength for Ap stars.

Mullan (1979) argued that if a spot were surrounded by oppositely directed magnetic fields, then the measured magnetic field would be much smaller than the real field strength. Robinson (1980) showed that this problem could be circumvented by measuring the changes in the widths of spectral lines, which was used by Robinson, Worden & Harvey (1980) to detect. magnetic fields on two cool stars *viz.* $\xi$ Boötis A (a G8 V star) and 70 Ophiuchi A (K0 B).

Marcy (1982) pointed out that this method relies upon the Zeeman–insensitive (i. e. $\pi$) and the Zeeman–sensitive (i. e. $\sigma_1$, $\sigma_2$) lines having the same profile.

Gray (1984) modelled the Zeeman profile $Z(\lambda)$ as an unshifted ($\pi$) component of relative intensity $I_p = \frac{1}{2}(1-\cos^2\theta)$ and shifted ($\sigma_1$, $\sigma_2$) components of relative intensity $I_s = \frac{1}{4}(1+\cos^2\theta)$, with $\theta$ being the angle between the line–of–sight and the magnetic fieldlines. If $A_0$ is defined so that $A_0 = \frac{1}{2}(1+\cos^2\theta)$, then

$$I_p = 1 - A_0$$

and

$$I_s = \frac{A_0}{2}.$$

His next stage was to perform a Fourier transform on $Z(\lambda)$. The Fourier transform of $Z(\lambda)$ is

$$z(\sigma) = 1 - A_0 + A_0 \cos(2\pi\sigma\Delta\lambda_1),$$

where $\Delta\lambda_1$ is the wavelength shift for the $\sigma_1$ and $\sigma_2$ lines. Then, if $I_\nu^0(\lambda)$ is the specific intensity of the line profile in the absence of magnetic fields, $I_\nu(\lambda)$, the intensity profile in the presence of the magnetic field, is given by a convolution:

$$I_\nu(\lambda) = I_\nu^0(\lambda) * Z(\lambda). \tag{1.1}$$

Using this, Gray (1984) was able to measure magnetic fields on 7 solar-type stars, *viz.* $\xi$ Boötis A (G8V), $\tau$ Ceti (G8V), $\sigma$ Draconis (K0V), $\epsilon$ Eridani (K2V), 70 Ophiuchi A (K0V), $\pi^1$ Ursae Majoris (G0V) and 61 Virginis (G6V).

## 1.4 Prominences

The first recorded occidental observation of solar prominences was by Birgerus Vassenius from Goteborg in 1733 (Pettit 1943). During a total solar eclipse, the apparent angular diameter of the Moon is greater than that of the Sun. During the July 1851 eclipse, observers near the northern edge of the track of totality saw prominences near the northern limb of the Sun which were invisible (i. e. hidden by the Moon) for observers near the southern edge of the track of totality, and similarly, observers near the southern edge of the track of totality saw prominences near the southern limb of the Sun which were invisible for observers near the northern edge of the track of totality. Moreover, prominences were seen to be fixed with respect to the Sun. Both these facts indicate that prominences are linked with the Sun rather than the Moon (Council of the Royal Astronomical Society 1852). Observations of that eclipse also showed that for observers near the northern (southern) edge of the track of totality, the corona appeared broader and brighter at the northern (southern) limb of the Sun than at the southern (northern) limb, indicating that the corona too was associated with the Sun (Council of the Royal Astronomical Society 1852). However, with the July 1860 eclipse, some observers (e. g. A. Billerbeck observing from

Rastenburg and Lt. F. A. Oom observing from Alto d'Urbuneja) said that before totality, the corona appeared concentric with the Moon (Raynard 1879).

Lockyer (1903) noted that– unlike spots– the centres of prominence activity could appear at high latitude. He also noted that the corona was irregular in shape when observed at total solar eclipses near sunspot maximum.

Lockyer & Lockyer (1903) investigated whether there was a link between prominence and sunspot activity. They noticed that the frequency of prominences within 40° of the solar equator appeared to vary in step with the sunspot cycle, with the number of such promincences peaking near sunspot maximum. However, those more than 40° from the equator showed no connection with the sunspot cycle, showing short outbursts of activity. Barocas (1939) also divided the prominences into two groups depending upon latitude. The low–latitude ones were those within 40° of the solar equator, and the high–latitude ones were those more than 40° from the solar equator. He found that the low–latitude prominences tended to exist between 18 and 28° from the equator, reaching the maximum latitude around sunspot minimum, whereas the high–latitude prominences were nearest to the poles around sunspot maximum.

Pettit (1939) suggested that it would be possible to determine the temperature of a solar prominence by comparing the widths of lines in the spectrum with those obtained from terrestrial sources. Using this technique, he determined a temperature of $\sim$7200K for one prominence.

Roberts (1948) used observations of an active solar prominence of June 1947 to suggest it was associated with the corona.

Pikel'ner (1971) argued that prominences were linked with thermal instabilities in the corona, and suggested that they could be caused by magnetic flux tubes starting in active regions. He argued that if the temperature decreased along the tube, then the thermal conduction will drop and a prominence could form. Priest & Smith (1979) showed that if the tube was stretched enough then a point would be reached where the thermal conduction could no longer keep the plasma thermally stable and cooling would follow. Priest, Hood & Anzer (1989) investigated twisting flux tubes in the corona, and showed that such a flux tube could produce a dip in the magnetic field, enabling a prominence to form and be supported against gravity– they suggested condensation in the corona as a suitable process. They also suggested that the necessary twisting could be caused by differential rotation. Dahlburg, Antiochos & Klimchuk (1998) investigated

prominence formation by localised heating, and suggested that chromospheric plasma is heated and evaporated into pre–existing prominence loops, after which it condenses into the growing prominence mass. Poland & Mariska (1986) suggested that if the parts of a flux tube nearest to the surface were heated, then additional material could be evaporated and end up trapped in the prominence.

Antiochos & Klimchuk (1991) commented that there seemed to be two contradictory requirements– the heating needed to increase (to increase the amount of material being evaporated from the surface) and to decrease (to form a condensation). They suggested that a heating increase had to be non–uniform, with the footpoints being heated more than the loop midpoint.

Solar prominences can be divided into two basic types (Priest 1984, Zirin 1988):

1. *Quiescent prominence:* These are stable, and can last for several months. These form on the timescale of about a day. They tend to form in regions of open magnetic field. These can be subdivided into:
   - Prominences in active regions.
   - Prominences in quiet regions.
   - Ascending prominences.
2. *Active prominence:* These occur in active regions, and are normally related to solar flares. These can be subdivided into:
   - Limb flares.
   - Loops and coronal rain.
   - Surges.
   - Sprays.

Prominences are seen around other stars as well as the Sun. Prominences can be observed as features in the H$\alpha$ profile (Collier Cameron & Robinson 1989a; Collier Cameron & Robinson 1989b; Collier Cameron 1999). Collier Cameron & Woods (1992) reported prominences around 4 stars in the $\alpha$ Persei cluster, *viz.* He373, He 520, He622 and He699, with prominences concentrated just outside the corotation radius. Byrne, Eibe & van den Oord (1998) reported

prominences around AB Doradûs, HK Aquarii, BD+22° 4409 and REJ1816+541. Wolk & Walter (1996) found an inverse P Cygni line profile in H$\alpha$ for V836 Tauri, which they explained as absorption of infalling material. Walter (1999) showed that discrete infall events are seen as transient redshifted absorption features in H$\alpha$.

If $\check{r} = r \sin\theta$ is the distance of the prominence from the rotation axis, $i$ the inclination of the rotation axis to the line of sight, $\omega$ the angular velocity of the star and $\dot{v} = \omega^2 \check{r} \sin i$ the drift rate of the prominence when crossing the centre of the stellar disk, then

$$\frac{\check{r}}{R_*} = \frac{\dot{v}}{v\omega \sin i} \tag{1.2}$$

(Collier Cameron 1999).

### 1.4.1 The Kippenhahn–Schlüter model

One of the early models for prominences was the *Kippenhahn–Schlüter model* (Kippenhahn & Schlüter 1957), which is explained in Priest (1984).

Using local Euclidean co–ordinates the prominence is modelled as a slab in the $y$–direction, where the $x$– and $y$–axes are parallel to the surface and the $z$–axis is perpendicular to the surface. It is assumed that the only variations are in the $x$–direction, so that

$$\frac{\partial}{\partial y} = \frac{\partial}{\partial z} = 0. \tag{1.3}$$

It is assumed that the magnetic field can be expressed as

$$\mathbf{B} = (B_X, B_Y, B_Z(x)). \tag{1.4}$$

It is also assumed that the temperature, pressure and density can be represented as

$$T = T_0, \tag{1.5}$$

$$p = p(x) \tag{1.6}$$

and the ideal gas law

$$\rho(x) = \frac{mp(x)}{k_B T}. \tag{1.7}$$

The divergence and curl of $\mathbf{B}$ are:

$$\nabla.\mathbf{B} = \frac{\partial B_Z}{\partial z} = 0 \tag{1.8}$$

and

$$\nabla \times \mathbf{B} = (0, -\frac{\partial B_Z}{\partial x}, 0). \tag{1.9}$$

The force balance is

$$0 = -\nabla p - \rho g \hat{\mathbf{z}} - \nabla \left(\frac{B^2}{2\mu}\right) + (\mathbf{B}.\nabla)\mathbf{B}\frac{1}{\mu} \tag{1.10}$$

The $x$– and $z$–components of 1.10 give

$$0 = \frac{d}{dx}\left(p + \frac{B^2}{2\mu}\right) \tag{1.11}$$

and

$$\frac{B_X}{\mu}\frac{dB_Z}{dx} = \rho g. \tag{1.12}$$

1.11 can be integrated to get

$$p(x) + \frac{B^2}{2\mu} = c, \tag{1.13}$$

where $c$ is a constant to be determined from the boundary conditions.

The boundary conditions are that as $x \to \pm\infty$ then $p(x) \to 0$ and $B_Z(x) \to \pm b_Z$.

Let $x \to \infty$ so that 1.13 gives

$$\frac{B_X^2 + B_Y^2 + b_Z^2}{2\mu} = c \tag{1.14}$$

This value for $c$ can be substituted into 1.13, giving

$$p(x) + \frac{B_X^2 + B_Y^2 + B_Z^2}{2\mu} = \frac{B_X^2 + B_Y^2 + b_Z^2}{2\mu},$$

which, with some cancelling of like terms, gives

$$p(x) = \frac{b_Z^2 - B_Z^2}{2\mu}. \tag{1.15}$$

The pressure scale height, $\Lambda$ is given by

$$\Lambda = \frac{k_B T_0}{mg},$$

so

$$\frac{m}{k_B T_0} = \frac{1}{\Lambda g}$$

which can be subsituted into 1.7 to give

$$\rho = \frac{p}{\Lambda g}.$$

Rearranging gives

$$p = \Lambda \rho g \tag{1.16}$$

So, from 1.15 and 1.16,

$$\rho g = \frac{b_Z^2 - B_Z^2}{2\Lambda\mu}. \tag{1.17}$$

The LHS of 1.17 is the same as the RHS of 1.12, so

$$\frac{B_X}{\mu}\frac{dB_Z}{dx} = \frac{b_Z^2 - B_Z^2}{2\Lambda\mu}, \tag{1.18}$$

which is a first order differential equation in $B_Z$, with solution

$$B_Z = b_Z \tanh \frac{b_Z x}{2B_X\Lambda}. \tag{1.19}$$

From 1.15

$$p(x) = \frac{b_Z^2}{2\mu}\operatorname{sech}^2\frac{b_Z x}{2B_X\Lambda}. \tag{1.20}$$

Equations 1.5 and 1.7 give the density

$$\rho(x) = \frac{b_Z^2 m}{2k_B T_0 \mu}\operatorname{sech}^2\frac{b_Z x}{2B_X\Lambda}. \tag{1.21}$$

The equations of the fieldlines can be determined from

$$\frac{dx}{B_X} = \frac{dz}{B_Z},$$

giving

$$\frac{dz}{dx} = \frac{B_Z}{B_X}.$$

From equation 1.19,

$$\frac{dz}{dx} = \frac{b_Z}{B_X} \tanh \frac{b_Z x}{2B_X \Lambda},$$

hence

$$z = \int \frac{b_Z}{B_X} \tanh \frac{b_Z x}{2B_X \Lambda} dx. \tag{1.22}$$

This can be integrated to give

$$z = 2\Lambda \log_e \left( \cosh \frac{b_Z x}{2B_X \Lambda} \right) + c, \tag{1.23}$$

where $c$ is a constant for each individual fieldline.

Anzer (1969) investigated the stability of prominences. He modelled a prominence as a current sheet of infinitessimal thickness lying along the $z-$axis, lying in a potential field, with variables depending only upon $x$ and $z$. If $[f]$ is the jump of a function $f(x,z)$ across a plasma–vacuum boundary then the necessary and sufficient conditions for stability are:

$$[B_z] \frac{dB_x(0,z)}{dz} \geq 0 \tag{1.24}$$

and

$$B_x(0,z) \frac{d[B_z]}{dz} \leq 0. \tag{1.25}$$

Priest (1984) showed that these can be written as

$$J \frac{dB_{x,0}}{dz} \geq 0 \tag{1.26}$$

and

$$B_{x,0} \frac{dJ}{dz} \leq 0 \tag{1.27}$$

respectively, where $J$ is the current flowing (in the $z-$direction) along the prominence.

If a prominence is supported solely by the Lorentz force, then

$$\rho g = B_{x,0} J, \tag{1.28}$$

which, when differentiated with respect to $z$, gives

$$g\frac{d\rho}{dz} = J\frac{dB_{x,0}}{dz} + B_{x,0}\frac{dJ}{dz}. \tag{1.29}$$

The first term on the RHS of equation 1.29 is non-negative (equation 1.26) and the second term on the RHS of equation 1.29 is non-positive (equation 1.27). Hence, there is no restriction on the sign of the LHS of equation 1.29, implying that $\frac{d\rho}{dz}$ could be positive or negative, i.e $\rho$ could increase or decrease with height.

The LHS of equation 1.28 is non-negative, implying that the RHS has to be as well, i.e.

$$B_{x,0}J \geq 0.$$

This can be multiplied by equation 1.27 to give

$$B_{x,0}^2 J\frac{dJ}{dz} \leq 0$$

$$\Rightarrow B_{x,0}^2\left(\frac{1}{2}\frac{dJ^2}{dz}\right) \leq 0,$$

giving

$$\frac{dJ^2}{dz} \leq 0, \tag{1.30}$$

since $\frac{1}{2}B_{x,0}^2 \geq 0$. Hence, in a stable prominence, $J$ cannot increase with height.

## 1.5 Chromospheric activity, X–ray flux and CaII H & K emission

### 1.5.1 X–ray flux

Ayres & Linsky (1980) noted from a sample of stars ranging from spectral type F4 to M0, and of luminosity classes III to V that $\frac{L_X}{L_{bol}}$ (where $L_X$ is the X–ray luminosity and $L_{bol}$ the bolometric luminosity) increased as the rotation period increased.

Pallavicini et al. (1981) investigated whether there was a relationship between $L_X$, $L_{bol}$ and $v\sin i$, using X–ray observations from the EINSTEIN Observatory. They found that:

- For O3–B5 stars $L_X \propto L_{bol}$.

- For A9–F8 stars $L_X \propto (v \sin i)^{\frac{1}{2}}$.
- For F7–M5 stars of luminosity classses III, IV and V, $L_X \propto (v \sin i)^{1.9 \pm 0.5}$. They suggested this could be connected with these stars having subphotospheric convection zones, which would have the capability of sustaining dynamo mechanisms. Subphotospheric convection zones are expected for main sequence stars with $T_{eff} \lesssim 8000$K (Schmitt et al. 1985).

Walter (1981) used a sample of F8–G5 stars of luminosity classes III, IV and V and found that the best straight–line fit was of the form

$$\frac{L_X}{L_{bol}} \propto \Omega^{1.2 \pm 0.3},$$

which disagrees with the result of Pallavicini et al. (1981).

From this, Walter (1981) suggested that the correct relation would be of the form

$$\frac{L_X}{L_{bol}} \propto \Omega f(d_{conv}),$$

where $f(d_{conv})$ was a function of the depth of the convective zone relative to the stellar radius. He argued that this would lead to the level of activity being dependent only on $\Omega$ and $T_{eff}$.

Walter (1982) looked for a relationship between $\frac{L_X}{L_{bol}}$ and $\Omega$, arguing that simply using $L_X$ would mean that one would be looking at the integrated surface X–ray flux, and a small star with a large proportion of its surface covered with active regions could have a similar value of $L_X$ as a large star with a small proportion of its surface covered with active regions, so he suggested using the relative surface flux $\frac{L_X}{L_{bol}}$, but commented that for stars of the same spectral type and luminosity class, $L_X$ and $\frac{L_X}{L_{bol}}$ are equivalent. He also decided to use $\Omega$, as rotational periodicities (and hence the angular velocity) can be determined from Ca II H and K flux variations (Stimets & Giles 1980) whereas the radius and inclination would be needed to determine $v$. Thus Walter (1982) decided to look at relations of the form

$$\frac{L_X}{L_{bol}} \propto \Omega^n.$$

Investigating a sample of F8–G2 stars, of luminosity class V, Walter (1982) tried to find a straight line fit to the data of the form

$$\frac{L_X}{L_{bol}} = A + B \log \Omega,$$

and found $A = -2.64 \pm 0.41$ and $B = 2.51 \pm 0.44$. However he found better fits of $A = -3.16 \pm 0.17$, $B = 1.21 \pm 0.22$ when $P < 1.05^d$ and $A = -1.25 \pm 0.61$, $B = 3.83 \pm 0.61$ when $P > 0.6^d$.

He suggested that the discrepancies in the power–law relationships found by Walter (1981) and Pallavicini et al. (1981) could be due to selection effects. He argued that one single power–law was insufficient to fit the data, and there was a discontinuity at $P \sim 12^d$, and commented that from the Skumanich relation (Skumanich 1972) this would correspond to an age of $\sim 10^9$ years, where the Vaughan–Preston gap (Vaughan 1980,Vaughan & Preston 1980) occurs.

Walter (1983) investigated F–type stars in more detail. He looked for a relation of the form

$$\log \frac{L_X}{L_{bol}} = A + B \log(v \sin i),$$

and only found a good ($\geq 0.7$) correlation for stars with (B-V)$\geq$0.46. He found that for (B-V)$\geq$0.52, $L_X \propto (v \sin i)^{1.3 \pm 0.2}$. He interpreted these results as indicating that F–type stars with (B-V)$\geq$0.46 had a solar–type dynamo. He suggested that either the structure of the differential rotation changed dramatically at this point, or that there is a critical convection zone depth needed for the dynamo.

One effective method of studying the effects of age on X–ray luminosity is to use open clusters, which would be composed of stars of similar age and chemical composition (Randich & Schmitt 1995).

Micela et al. (1985) assumed that $L_X \propto (v \sin i)^2$ for G dwarfs and compared $\langle L_X \rangle$ for G dwarfs in the Hyades and the Pleiades. They found that for the Pleiades the value was $10^{29.6 \pm 0.1}$erg s$^{-1}$ whereas for the Hyades it was lower, $10^{29.1 \pm 0.1}$erg s$^{-1}$. They interpreted this as evidence that, for stars of similar spectral type, $L_X$ decreases with age.

Maggio et al. (1987) also used the EINSTEIN Observatory to study F7–G9 stars of luminosity types IV and V, within 25pc of the solar system, and calculated the X–ray luminosity, $L_X$, to be

$$\log L_X = 39.9 + 2.54 \log R'_{HK}, \tag{1.31}$$

where $L_X$ is in erg s$^{-1}$. They argued that the good correlation (correlation coefficient of 0.84) would be due to $L_X$ and $R'_{HK}$ having a common origin, and so looked for a connection between

$L_X$ and the surface rotation velocity $v$, obtaining

$$\log L_X = 2.1 \log v + 26.5, \tag{1.32}$$

where $v$ is in km $s^{-1}$. They argued that this result was in good agreement with that of Pallavicini et al. (1981), and that this implied that the $L_X$–$v$ relation for F7–G9 stars was independent of spectral type.

Micela et al. (1988) used EINSTEIN observations of the Hyades to investigate $L_X$. They found that for main sequence G–type stars

$$\langle \log L_X \rangle = 29.16^{+0.05}_{-0.07},$$

confirming the decrease of $\langle L_X \rangle$ with age found by Micela et al. (1985). Micela et al. (1988) found a similar trend for main sequence K–type stars, although G and K–type stars had different X–ray luminosity distributions, indicating that $L_X$ depends on $(B - V)$ as well as age.

Randich & Schmitt (1995) used ROSAT observations of Praesepe, which is of a similar age to the Hyades (from HIPPARCOS data Robichon et al. (1997) determined the age of Praesepe to be ~830 Myr, and Lebreton et al. (1997) determined the age of the Hyades to be 625±100 Myr), and found a lower detection rate in X–rays (33% for dG, 14% for dK and 13% for dM) than for the Hyades. They interpreted this as meaning that Praesepe stars appeared as a whole to be intrinsically less luminous in X–rays than their Hyades counterparts. Barrado y Navascués, Stauffer & Randich (1998) investigated this difference between the Hyades and the Pleiades, but were unable to draw any firm conclusions, and suggested that further observations of open clusters of a similar age were needed.

Randich, Schmitt & Prosser (1996) studied the Coma Berenices cluster, which is of a similar age (~430 Myr) as the Hyades and Praesepe (Boesgaard 1989). However, it has a lower proportion of late–type main sequence stars than the Hyades and Praesepe. Another major difference is that the Hyades and Praesepe both have high metallicities (*viz.* [Fe/H]=0.125±0.032) and Coma has a low metallicity of [Fe/H]=-0.082±0.039 (Boesgaard 1989). Friel & Boesgaard (1992) commented that these three clusters would preserve the inhomogeneities of the gas they formed from.

Randich, Schmitt & Prosser (1996) noted that the X–ray detection rate for Coma was closer to that for the Hyades than for Praesepe, and the X–ray luminosity distribution functions

for G–type stars in the Hyades and Coma were similar. They argued that if $L_X$ depended upon metallicity, then it would be expected that it would be the Hyades and Praesepe which were similar, and Coma different.

They suggested that there could be a difference in the distribution of the rotational velocity, but, if this were the case, there would be the problem as to why there were different rotational velocity distributions in clusters of a similar age.

Randich et al. (1995) studied the open cluster IC 2602, which is only 36 Myr old (Mermilliod 1981). They found that the value of $\frac{L_X}{L_{bol}}$ saturated at $(B-V) \sim 0.7$, and at later spectral types, the maximum value of $L_X$ ($L_{X,max}$) decreased. They compared the X–ray luminosity distribution function with that for the Pleiades, and found that for $(B-V) > 1.25$ they were similar, but for $(B-V) < 1.25$, the IC 2602 stars appeared to have a higher $L_X$ than for the Pleiades. They suggested that this could mean that when a star evolves between 30 and 70 Myr, there is a significant decrease in $L_X$ with age for the stars with $(B-V) < 1.25$, but $L_X$ remains more–or–less the same for stars with $(B-V) > 1.25$.

They suggested that if open clusters followed a similar evolution of rotational velocity, then one would expect the G and early K dwarfs in IC 2602 to rotate faster in general than those in the Pleiades, and if there was a strong link between rotational velocity and $L_X$ then these stars in IC 2602 would have a higher $L_X$ than those in the Pleiades, as is observed. They claim that this indicates a link between age and $L_X$.

Stauffer et al. (1997) also observed IC 2602, and compared it with IC 2391, which is of a similar age. They noted that $\frac{L_X}{L_{bol}}$ saturates for rapid rotators, but the saturation level declined for $v \sin i \gtrsim 100$ km s$^{-1}$, a supersaturation effect noticed in the $\alpha$ Persei cluster by Prosser et al. (1996).

Schmitt et al. (1990) investigated the Ursa Major stream, and found no correlation between $L_X$ and $v \sin i$, but they argued this could be due to the small sample (18 stars).

Vilhu (1984) investigated the saturation of $\frac{L_X}{L_{bol}}$ and suggested that this was due to the disc being totally filled with active regions, but Jardine & Unruh (1999) noted that if the rotation rate is increased, then the density and the pressure would increase in the outer corona, where the largest magnetic structures would lie, and the corotation radius would move inwards. They

suggested centrifugal stripping of the corona as the cause of the saturation.

James et al. (2000) studied rotation rate and $L_X$ for M–dwarfs, to investigate the super-saturation observed by Prosser et al. (1996) and Stauffer et al. (1997). They found tentative evidence for supersaturation.

Schrijver (1983) investigated whether there was a correlation between the soft X–ray flux density at the surface ($F_X$) and the Ca II H & K line–core flux density($F_{HK}$). Setting $\Delta F_{HK}$ to be the excess Ca II H & K flux, which is the flux above the *basal flux* (Schrijver 1987)– a lower limit which depends on (B-V) and luminoisty class. He found that

$$F_X \propto \Delta F_{HK}^{1.67}. \tag{1.33}$$

### 1.5.2 Ca II H & K flux and H$\alpha$ emission

Huggins & Huggins (1897) investigated the behaviour of calcium at low density, such as high up in the chromosphere, intending to find out under what conditions the H and K lines dominated. They slowly reduced the density of a calcium vapour, and examined the spectrum, finding that the other lines reduced in strength compared to the H and K lines as the density was decreased.

Eberhard & Schwarzschild (1913) noted that $\alpha$ Boötis, $\alpha$ Tauri and $\sigma$ Geminorium all showed Ca II K emission, and suggested that this could be due to solar–like activity.

Babcock & Babcock (1955) noticed that there was a strong correspondence between solar regions showing Ca II flocculi and bipolar magnetic regions, with Ca II plages being associated with those bipolar regions with a magnetic field $\gtrapprox$2G. This work was extended by Frazier (1970) who noted that there were *downdrafts*– isolated regions of downflowing material– at the edges of the supergranules, which were highly correlated with Ca II K emission. Skumanich, Smythe & Frazier (1975) also noticed a linear correlation between magnetic field strength and Ca II K emission, and suggested that Ca II K emission could be used to measure chromospheric activity on other stars.

Leighton (1959) observed the structure of the azimuthal field on the Sun, and noticed that there was a strong correlation between the field pattern and the structure of Ca II emission. He suggested that all Ca II emission was associated with magnetic fields. Howard (1959) also noticed a strong correspondence between magnetic fields and Ca plage regions.

Wilson & Bappu (1957) investigated whether the emission line width for Ca II H and K lines depended upon

1. emission intensity,
2. stellar luminosity and
3. spectral type.

They studied stars later than G0, and found that for Ca II K the only dependence was upon the stellar luminosity, with a linear relation between the absolute magnitude $M_V$ and the logarithm of the width of the emission line. They suggested that this relationship provided a method of determining the intrinsic luminosity of late–type stars. They argued that the width cannot depend upon the surface gravity, and suggested that turbulent motion within the emitting chromosphere could cause the lines to broaden due to the Doppler effect. This was further calibrated by Wilson (1959) using the Sun and four K–type giants in the Hyades ($\gamma$, $\delta$, $\epsilon$ and $\theta^1$ Tauri).

Wilson (1963) noted from comparisons of CaII H & K emission in main sequence stars in open clusters (the Pleiades, the Hyades, Praesepe and the Coma Berenices cluster) and field stars that the younger stars appeared in general to have stronger emission, and suggested that this was connected with the strength of the magnetic field. Wilson & Skumanich (1964) suggested that, for single stars later than F7, the strength of Ca II H and K emission was an indicator of the star's age.

Skumanich (1972) noted that– for the small sample he used– the rotation rate was proportional to the Ca II emission, and suggested that both decayed as the inverse square root with time. This was consistent with Weber & Davis (1967) who from modelling the solar wind, argued that the angular momentum of the Sun, $J$, would evolve as

$$\dot{J} \propto \Omega \dot{M}, \tag{1.34}$$

equivalent to

$$\dot{J} = -\frac{J}{\tau}, \tag{1.35}$$

where $\tau$ is a characteristic timescale (for the Sun $\sim$ 7x10$^9$years).

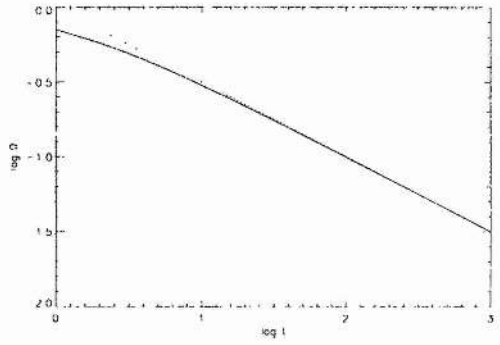

Figure 1.1: The solid line shows a solution to equation 1.38 where $\Omega_0$=1 and $\gamma$=1, and $t$ going up to 1000. The dotted line is for $\Omega \propto t^{-\frac{1}{2}}$

Li & Collier Cameron (1993) showed that this gives

$$\dot{\Omega} \propto -B_0^2 \Omega, \tag{1.36}$$

which, when there is a linear dynamo law $B_0 \propto \Omega$, leads to

$$\dot{\Omega} \propto -\Omega^3. \tag{1.37}$$

From 1.37

$$\Omega = \Omega_0 \left[1 + \gamma \Omega_0^2 (t - t_0)\right]^{-\frac{1}{2}}, \tag{1.38}$$

where $\Omega_0$ is the angular momentum at time $t_0$ and $\gamma$ is a constant.

1.38 can also be written as

$$\left(\frac{1}{\Omega^2} - \frac{1}{\Omega_0^2}\right) \propto (t - t_0). \tag{1.39}$$

with a positive constant of proportionality, so if $\Omega \to \infty$ as $t \to t_0$, then we get $\Omega \propto t^{-\frac{1}{2}}$, as shown in figure 1.1.

However, Soderblom et al. (1993) argued that the Skumanich model was too simple, as it failed to tackle UFRs (Ultra Fast Rotators) adequately and didn't explain the mass–dependent rotation distribution found in the Hyades.

Sheeley (1967) noted that the Ca II K emission in the solar chromosphere varies with the sunspot cycle, by about 40%, a result later confirmed by White & Livingston (1981). Sheeley

(1967) identified this as being due to a greater area of the solar disc being covered in flocculi (which have a greater intensity of Ca II K emission than other parts of the disc) and noted that if the Sun were observed from a large enough distance so that it appeared to be a point source, then an observer would simply notice that the Ca II K emission were varying. He suggested that observing Ca II K emission from stars would indicate whether they had a noticeable activity cycle. Wilson (1968) noted that the change in solar luminosity is less than 0.001 mag, so looking at luminosity variations in solar–type stars would not be a practical method for investigating activity cycles.

Wolff, Boesgaard & Simon (1986) investigated F–type stars, finding that chromospheric activity (measured by the He I line) started at (B-V)≈0.28, corresponding to spectral type ∼F0. They argued that the disappearance of Ca II H and K emission lines around type F4–5 (Wilson 1966) is due to a loss of contrast between the emission and the photospheric background.

The Mount Wilson project (Wilson 1978; Vaughan, Preston & Wilson 1978) studied the Ca II H and K emission lines of 91 main–sequence stars, ranging from spectral types F5 to M2. The Mount Wilson project led to a catalogue of 65263 observations of 1296 stars (Duncan et al. 1991).

The flux measurements at the Ca II H and K emission wavelengths were taken in 1Å bands and calibrated with two 25Å–wide reference bands. The aim was to see whether the chromospheric activity of main–sequence stars showed any temporal variation, and if they did, how they varied.

Wilson (1978) also noted short term (∼days) variation, and that the standard deviation of these variations was proportional to the total Ca II H and K emission. This was confirmed by Vaughan et al. (1981).

Vaughan, Preston & Wilson (1978) defined a *flux index*, $S$, for each star by

$$S = \alpha \frac{N_H + N_K}{N_V + N_R}, \tag{1.40}$$

where $\alpha$ is a normalising factor, $N_H$ and $N_K$ are the number of counts (corrected for the sky background) in the H– and K–bands and $N_V$ and $N_R$ are the counts in the two reference bands.

Vaughan & Preston (1980) surveyed 486 main sequence field stars, of spectral types F through to M, all within 25pc of the Sun, and plotted $\log S$ against $(B - V)$, and were able to

classify the sample stars into 4 groups:

- dMe stars,
- late K and M type stars (1.1≤(B-V)≤1.6), nearly all showing strong Ca II emission,
- chromospherically very active F and G type stars,
- less active F and G type stars– the Sun would be in this group (Vaughan 1980).

Vaughan & Preston (1980) suggested that the gap between the third and fourth groups (the *Vaughan–Preston gap*) could be simply due to sampling, or alternatively, it could be a sign that chromospheric activity declines suddenly at around $10^9$yr.

Vaughan (1980) investigated the Vaughan–Preston gap in more detail, using a new sample of F and G main sequence stars (albeit with some overlap with the previous sample), and looked at the two branches of the F and G type stars, using the variations in the Ca II H and K emission lines observed by Wilson (1978). He noted that the stars on the lower branch had regular cycles, whereas those on the upper branch appeared to vary in emission chaotically.

Vaughan (1980) used the fact that chromospheric activity decreases as stars age (Wilson 1963;Wilson & Skumanich 1964;Skumanich 1972) to suggest that the stars on the upper branch were younger than those on the lower. By comparison with the Sun, he suggested that the variation in intensity of the Ca II H and K emission lines for the lower branch stars were due to calcium plages which were associated with regions which were magnetically active.

The convective turnover time, $\tau_c$ can be calculated by

$$\tau_c = \begin{cases} 5.2 + 53((B-V) - 0.50) & \text{if } 0.5 \leq (B-V) \leq 0.79 \\ 20.5 & \text{if } 0.79 \leq (B-V) \leq 1.4 \end{cases} \tag{1.41}$$

(Stępień 1989)

The *Rossby number*, *Ro*, is a dimensionless number given by

$$Ro = \frac{P_{rot}}{\tau_c(B-V)}. \tag{1.42}$$

Noyes et al. (1984) found that, for the stars observed in the Mount Wilson project, the mean level of Ca II H and K emission was correlated with $P_{rot}$, the rotation period. They defined

$R'_{HK}$ to be the ratio of the emission in the cores of the Ca II H and K lines to the total bolometric emission, and investigated whether there was a relation between the mean value $\left\langle R'_{HK} \right\rangle$ and the observed rotation period $P_{obs}$ of the star. They found that plotting the data produced large scatter, but this could be reduced by plotting $\left\langle F'_{HK} \right\rangle$ against $P_{obs}$, where $F'_{HK} = \sigma R'_{HK} T_{eff}^4$.

However, plotting $\left\langle R'_{HK} \right\rangle$ against $Ro$ produced a relationship where $R'_{HK}$ increased for decreasing $Ro$, with the rate of change being larger for large values of $Ro$. They suggested this could be due to saturation of the Ca II H and K emission. This need not mean that the underlying dynamo is being saturated– Jardine & Unruh (1999) showed that the observed saturation of X–ray emission could be explained by the centrifugal stripping of the corona with increasing rotation rate, as a star of solar mass would have the corotation radius inside the corona if it rotated faster than ∼2–3 days.

Surprisingly, Noyes et al. (1984) didn't find any evidence for the Vaughan–Preston gap.

Schrijver et al. (1989) investigated whether there was a link between the core emission of the Ca II K line and the photospheric magnetic field for the Sun. Considering $\langle f \rangle$– the hemisphere–averaged filling factor, and $B$–the mean magnetic field in flux tubes, they showed that

$$F_X \propto \langle fB \rangle^{0.90 \pm 0.10},$$

which, using equation 1.33 gives

$$\Delta F_{HK} \propto \langle fB \rangle^{0.62 \pm 0.14}.$$

They noticed that this only held for $\langle fB \rangle \lessapprox 300$G, and above that $\Delta F_{HK}$ saturates. They also found that if $I_c$ is the Ca II K line core intensity, and $I_w$ the Ca II K wing intensity, then

$$\Delta F_{HK} \propto \frac{\Delta I_c}{I_w}. \tag{1.43}$$

They found that the minimum $F_{HK}$ on the Sun– in regions of near–zero flux density– was similar to the lowest values of $F_{HK}$ found in the Mount Wilson survey. The suggested that this meant that the stars with the lowest values of $F_{HK}$ had small magnetic fields, hence were inactive. They found that for solar–type dwarfs, $\Delta F_{HK}$ saturates for $\langle fB \rangle \sim 300$G.

Herbig (1985) studied main sequence stars of spectral types F8–G3, and found that $F_{HK} \propto t^{-0.40 \pm 0.12}$, where $t$ is the time on the Main Sequence.

### 1.5.3 Lithium abundance and age for solar–type stars

Shima & Honda (1963) analysed chondrite meteorites, and determined $[N(\mathrm{Li})]/[N(\mathrm{Si})]$ to be $36\mathrm{x}10^{-6}$, and Mutschlecner (1963) determined $[N(\mathrm{Li})]/[N(\mathrm{Si})]$ in the solar atmosphere to be $1.1\mathrm{x}10^{-6}$. Herbig (1965) assumed that the replenishment of Lithium was negligible, and modelled the change in Lithium abundance as an exponential decay:

$$L(t) = L(0)e^{-\frac{t}{t_c}}. \tag{1.44}$$

Assuming that $L(t)$ is the Lithium abundance at time $t$, $L(0)$ was the Lithium abundance in the chondrite meteorites (which can be assumed to date from the formation of the Solar System), $t = 4.7\mathrm{x}10^9$ years is the age of the Solar System, and rearranging equation 1.44 as

$$t_c = \frac{t}{\log \frac{L(0)}{L(t)}}$$

gives

$$t_c = 1.32\mathrm{x}10^9 \mathrm{years}.$$

Greenstein & Richardson (1951) suggested that convection would deplete the Lithium abundance in the solar atmosphere.

Herbig (1965) noted that T Tauri stars were Lithium–rich compared to other dwarfs.

Wallerstein, Herbig & Conti (1965) studied the Lithium abundances for stars in the Hyades, investigating $[N(\mathrm{Li\ I})]/[N(\mathrm{Ca\ I})]$. They noticed that main–sequence Hyades stars had a higher Lithium abundance than the Sun had, and that there was a decrease in Lithium abundance for stars later than (B-V) $\simeq$ 0.61 (corresponding to spectral type G1V). They suggested this could be because stars of later spectral type have deeper convective zones.

Skumanich (1972) suggested that Lithium abundance decayed as $t^{-\frac{1}{2}}$.

Duncan (1981) investigated whether there was any link between Ca II K emission and Lithium abundance. He was able to subdivide his sample of F5–G5 dwarfs and subgiants into three groups:

- *Group A*. These had strong Ca II K emission and high Lithium abundance.

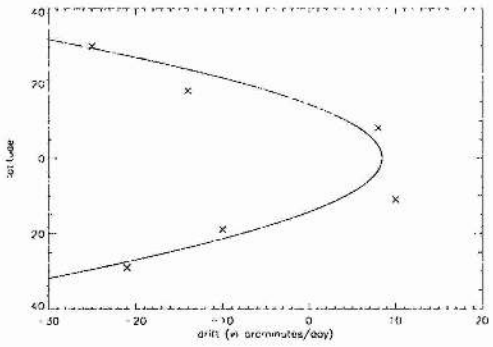

Figure 1.2: The solar differential rotation from Carrington (1859)

- *Group B.* These had weak Ca II K emission and low Lithium abundance.
- *Group C.* These had weak Ca II K emission and high Lithium abundance.

He suggested that for Group C stars, the method for Lithium depletion was inefficient.

One problem with measuring Lithium abundance, which was noticed by Giampapa (1984) is that chromospheric activity can alter the observed equivalent width of the 6707ÅLithium line, which affects the measurement of Lithium abundance.

## 1.6 Differential rotation

From his solar observations, Carrington (1858) noted that spots at different latitudes took different lengths of time to go round the Sun.

Carrington (1859) assumed a solar rotation period of 25.380 days, and measured the drift in longitude of features (in arcminutes per days) at 6 latitudes. From his results, the best fit is

$$d = 8.43607 - 138.240 \sin^2 \lambda, \tag{1.45}$$

where $d$ is the drift (in arcminutes per days) and $\lambda$ is the latitude.

This is plotted in figure 1.2.

Baliunas et al. (1985) suggested that for 4 of the stars (table 1.1) in the Mount Wilson project (Wilson 1978) the variations in the periods in different observing seasons could be caused by differential rotation.

| star | $m_V$ | spectral type |
|---|---|---|
| HD 101501 | 5.33 | G8V |
| HD 114710 | 4.26 | G0V |
| HD 190406 | 5.80 | G1V |
| HD 206860 | 5.94 | G0V |

Table 1.1: This table lists the stars suspected of differential rotation by Baliunas et al. (1985). The values of $m_V$ are from Hirshfield & Sinnott (1982). The spectral types are from Baliunas et al. (1985) and agree with those given by Hirshfield & Sinnott (1982). HD 101501 is 61 Ursae Majoris, HD 114710 is $\beta$ Comae Berenices and HD 190406 is 15 Sagittae.

Donahue, Saar & Baliunas (1996) pointed out that the mean rotation period as measured by starspots would decrease in period over an activity cycle if, like the solar case (Maunder 1913) the peak distribution of spots moves equatorwards as the cycle progresses. Busso, Scaltriti & Cellino (1985) observed differential rotation in 3 RS Canum Venaticorum systems, *viz.* SS Boötis, SV Camelopardalis and VV Monocerotis.

Donati & Collier Cameron (1997) found a relationship between surface rotation rate and latitude for AB Doradûs by tracking individual starspots.

## 1.7 Dynamo

Having described the various phenomena in the previous sections, we need to ask whether there is a way of unifying all of these into one theory. In particular, is there any connection between the cycle period $P_{cyc}$ of the magnetic activity, the rotation rate $P_{rot}$ and the convective turnover time $\tau_c$?

Vaughan et al. (1981) argued that long (~10–12 year) activity cycles in late–type main sequence stars were found among those with $P_{rot} \gtrsim 20$ days, and that the period of these cycles were uncorrelated with the equatorial rotational velocity.

Noyes, Weiss & Vaughan (1984) investigated slowly–rotating stars (with $P_{rot}$ of the order

of 1–2 months) below the Vaughan–Preston gap with spectral types G2 to K7 and found that

$$P_{cyc} \propto Ro^{1.25\pm0.5}.$$

Brandenburg, Saar & Turpin (1998) and Saar & Brandenburg (1999) looked at relating $P_{cyc}$ to more stellar properties. Brandenburg, Saar & Turpin (1998) argued that the ratio $P_{rot}/P_{cyc}$ varied as $t^{-0.35}$ up to an age of about 2–3x$10^9$ years, with older stars following a similar relationship but with the ratio $P_{rot}/P_{cyc}$ about 6 times greater than for younger stars.

## 1.8 AB Doradûs

AB Doradûs (also known as HD 36705 and SAO 249286) is a K0 dwarf, originally discovered as a bright X–ray source by Pakull (1981) and subsequently observed by ROSAT (Kürster et al. 1997), EUVE (Mewe et al. 1996), *Beppo*SAX (Maggio et al. 2000) and XMM–*Newton* (Güdel et al. 2001). Slee et al. (1986) observed 2 radio flares from it, each lasting about 3 days. It also is known to have Ca II H and K emission (Bidelman & MacConnell 1973).

Its photometric variability, of $\sim$ 0.09 in the $V$–band (Innis et al. 1985) is believed to be due to starspots (Anders 1990, Innis et al. 1988) and this, combined with its brightness ($V \simeq 7.0$) and rapid rotation (P=$0\overset{d}{.}514$) have made it an attractive candidate for Doppler imaging (Kürster, Schmitt & Cutispoto 1994, Collier Cameron & Unruh 1994, Collier Cameron 1995, Unruh, Collier Cameron & Cutispoto 1995).

According to HIPPARCOS data it is 14.94±0.12 pc away and it is $\sim$2–3x$10^7$yr old (Collier Cameron & Foing 1997). From observations of the Lithium line at 6708Å, Rucinski (1982) commented that the high Lithium abundance implied that it was a young star, and he suggested that it was a post–T Tauri star. Vilhu, Gustafsson & Edvardsson (1987) said that the Lithium abundance is equal to the primordial value of $\log n(\mathrm{Li}) \simeq 3$, (where $\log n(\mathrm{H}) = 11.95$) (Duncan 1981). Using extreme–UV observations, Mewe et al. (1996) showed that Iron, Oxygen, Magnesium, Silicon and Sulphur were all less abundant in AB Doradûs than in the Sun. From its galactic space velocity Innis, Thompson & Coates (1986) inferred that it was part of the Pleiades Group (Local Association).

It is assumed to be inclined at an angle of 60°(Kürster, Schmitt & Cutispoto 1994).

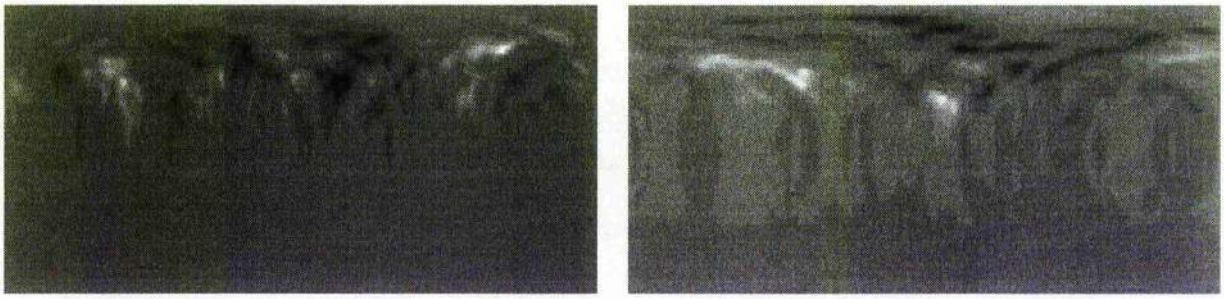

Figure 1.3: This diagram shows the observed radial (left) and azimuthal (right) fields for 1995.

It is of interest for a variety of reasons:

1. The most important, for the purposes of this thesis, is that Zeeman Doppler images have been obtained for 3 consecutive years

   (a) 11–13 Dec 1995 (Donati & Collier Cameron 1997)

   (b) 23,25 and 29 Dec 1996 (Donati et al. 1999)

   (c) 10–15 Jan 1998

   which reveal that the radial field has at least 12 regions of opposite polarities at intermediate to high latitude, which are approximately regularly spaced in longitude together with a unidirectional ring of azimuthal field at 70–80° indicating an underlying large–scale toroidal field (Donati et al. 1999). The observed radial and azimuthal fields for 1995 are given in figure 1.3, those for 1996 in figure 2.6 and those for 1998 in figure 1.4.

2. It has X–ray and radio emission (Collier Cameron & Robinson 1989a, Vilhu et al. 1993) including X–ray flares (Collier Cameron et al. 1988, Vilhu et al. 1993, Schmitt, Cutispoto & Krautter 1998). These flares have a mass of $\sim 10^{18}g$ and were observed about once per rotation period, and can be fitted either by thermal Bremstrahlung emission with $kT = 4.35$ KeV, or by a power–law spectrum with $\gamma \in (2.3, 2.6)$ (Vilhu et al. 1993). Lim et al. (1992) observed the radio emission to be rotationally modulated, and suggested this could be due to active starpsot regions. There is indirect evidence from radio observations at 3,6,13 and 20 cm that the radio emission is highly directive and suggests synchrotron radiation (Lim et al. 1994).

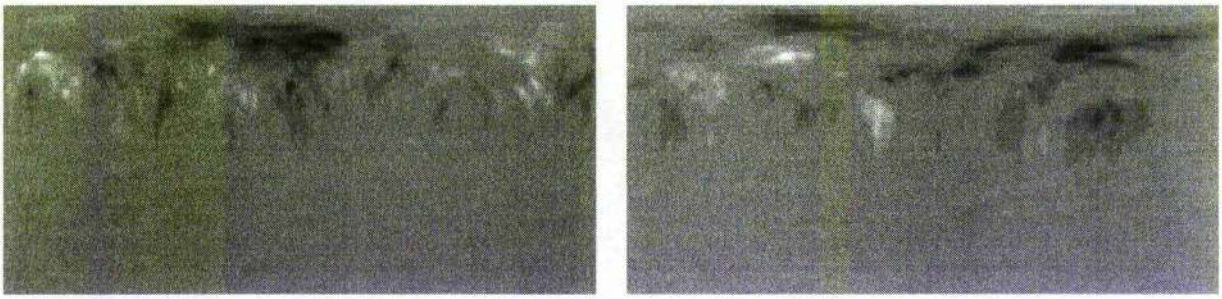

Figure 1.4: This diagram shows the observed radial (left) and azimuthal (right) fields for 1998.

3. It has circumstellar prominences which can be observed as absorption transients in optically thick low–excitation lines e.g. H Balmer, CaII and MgII when the prominences cross the line–of–sight (Collier Cameron & Robinson 1989a,Collier Cameron & Robinson 1989b. These prominences are trapped by the stellar magnetic field at, or beyond, the point of centrifugal balance, with Donati et al. (1999) showing there were about 16 prominence structures with lifetimes of less than 4 rotation periods, concentrated around $4R_*$. Jardine et al. (1998) reported prominences lying between 3.1 and $4.3R_*$. Their presence demonstrates that the corona is highly structured even as far out as 3–$5R_*$ (Jardine & Ferreira 1996).

4. Despite the rapid rotation, the differential rotation has been measured using these Zeeman Doppler images to be close to solar (Donati & Collier Cameron 1997), with the equator lapping the poles in $\sim 110^d$ (*cf.* $120^d$ in the solar case).

## 1.9 Aims

In this thesis I intend to

- To investigate whether there is a link between the differential rotation and the high latitude band of unidirectional azimuthal field.
- To investigate the effect of diffusion and differential rotation on the evolution of AB Doradûs's magnetic field. In particular, we want to determine the lifetime of surface magnetic

features based solely on these two processes. Barnes et al. (1998) have shown that the spot distribution of the similar young rapid rotator He699 becomes uncorrelated after 30 days. Is this timescale consistent with the effects of diffusion and differential rotation?

- To investigate the coronal topology of the field, and where stable prominences can exist. Do these points relate to places where prominences are known to exist, or is modelling the coronal field as a potential field from the observations insufficient?

CHAPTER 2

# The surface magnetic field of AB Doradûs

The work is this chapter will be appearing in Monthly Notices of the Royal Astronomical Society, "The Magnetic Field of AB Doradûs" by G. R. Pointer, M. Jardine, A. Collier Cameron and J.-F. Donati.

## 2.1 The Nature of the Magnetic Field

The Zeeman Doppler images provide, in principle, three vector components of the magnetic field at the stellar surface. From these we can determine how accurately the observed field can be approximated by a potential (i.e. current-free) field. For a force-free field, where the magnetic field dominates force balance, the current $\mathbf{j}$ flows along magnetic field lines and so, since $\mu\mathbf{j} = \nabla\times\mathbf{B}$, we have

$$\nabla\times\mathbf{B} = \alpha\mathbf{B} \tag{2.1}$$

where $\alpha = 0$ gives a potential field. In spherical co-ordinates (r,$\theta$,$\phi$) we can take the radial component of 2.1 and write $\alpha$ as

$$\alpha(r,\theta,\phi) = \frac{1}{R_* B_r \sin\theta}\left[\frac{\partial}{\partial\theta}(B_\phi \sin\theta) - \frac{\partial B_\theta}{\partial\phi}\right] \tag{2.2}$$

where $R_*$ is the stellar diameter. This allows us to calculate $\alpha$ across the surface from the actual observations. The other components of 2.1 are not suitable for determining $\alpha$ from the observations as they involve derivatives in the radial direction. Because of the lack of observational data over much of the south polar region, we decided to restrict our analysis to the northern hemisphere of AB Doradûs, where we define the northern pole to be that facing towards us.

If we assume that the field is potential, then we can write $\mathbf{B}$ in terms of a potential function $\psi$, with

$$\mathbf{B} = -\nabla\psi,$$

which in spherical co-ordinates gives

$$B_r = -\frac{\partial\psi}{\partial r},$$

$$B_\theta = -\frac{1}{r}\frac{\partial\psi}{\partial\theta}$$

and

$$B_\phi = -\frac{1}{r\sin\theta}\frac{\partial\psi}{\partial\phi}.$$

where $\psi$ satisfies Laplace's equation $\nabla^2\psi = 0$ which can be expressed as

$$\frac{1}{r^2}\frac{\partial}{\partial r}(r^2\frac{\partial\psi}{\partial r}) + \frac{1}{r^2\sin\theta}\frac{\partial}{\partial\theta}(\sin\theta\frac{\partial\psi}{\partial\theta}) + \frac{1}{r^2\sin^2\theta}\frac{\partial^2\psi}{\partial\phi^2} = 0. \tag{2.3}$$

A separable solution for $\psi$ can be found

$$\psi(r,\theta,\phi) = \sum_{l=1}^{N}\sum_{m=-l}^{l}\psi_{lm}(r)P_{lm}(\theta)e^{im\phi},$$

where $P_{lm}$ are the associated Legendre functions and

$$\psi_{lm}(r) = a_{lm}r^l + b_{lm}r^{-(l+1)}.$$

We chose to truncate the series at $N = 63$, corresponding to the maximum resolution of the reconstructed field images. We clearly need two boundary conditions to determine $\psi$. We chose to specify as one boundary condition that at some distance from the star (the *source surface*, $r_s \approx 5.1R_*$), the field is radial and so

$$B_\theta(r_s) = B_\phi(r_s) = 0 \tag{2.4}$$

(Schatten, Wilcox & Ness 1969). This mimics the stellar wind.

Since most stellar prominences form at around the corotation radius ($2.7R_*$), we know that a significant fraction of the field is closed at that radius. For this reason and for consistency with Jardine et al. (1999) we choose $r_s = 5.1R_*$.

We then have

$$a_{lm}r_s^{l-1} + b_{lm}r_s^{-l-2} = 0,$$

equivalent to

$$\psi_{lm} = 0.$$

As a second boundary condition we impose the radial field at the surface to be the observed radial field. We can then express the magnetic field in terms of the two-dimensional Fourier coefficients $B_{lm}$, where

$$B_{lm}(R_*) = 2\pi \int_0^\pi B_m(\theta) P_{lm}(\theta) \sin\theta d\theta$$

so

$$B_{lm}(R_*) = -l a_{lm} R_*^{l-1} + (l+1) b_{lm} R_*^{-l-2}$$

The function $B_m(\theta)$ is derived from a fast Fourier transform performed latitude-by-latitude on the observed radial field $B_r(R_*, \theta, \phi)$

Once the field is evolved due to diffusion and differential rotation, it is not necessarily potential, although it can still be expressed as a sum of spherical harmonics. The field components are then expressed in terms of the functions

$$J = \sum_{l=1}^{N} \sum_{m=-l}^{l} J_{lm} P_{lm}(\theta) e^{im\phi}$$

and

$$A = \sum_{l=1}^{N} \sum_{m=-l}^{l} A_{lm} P_{lm}(\theta) e^{im\phi}$$

where

$$J = \frac{1}{\sin\theta} \left[ \frac{\partial}{\partial\theta} (\sin\theta B_\phi) - \frac{\partial B_\theta}{\partial\phi} \right]$$

is the radial component of the current and

$$A = \frac{1}{\sin\theta} \left[ \frac{\partial}{\partial\theta} (\sin\theta B_\theta) + \frac{\partial B_\phi}{\partial\phi} \right]$$

is the 2-dimensional divergence.

## 2.2 Evolving the field using the induction equation

From three of Maxwell's equations

$$\nabla \times \mathbf{B} = \mu \mathbf{j},$$

$$\nabla.\mathbf{B} = 0,$$

$$\nabla\times\mathbf{E} = -\frac{\partial\mathbf{B}}{\partial t}$$

and Ohm's Law

$$\mathbf{j} = \sigma(\mathbf{E} + \mathbf{v}\times\mathbf{B}),$$

where $\sigma$ is the conductivity we get the induction equation

$$\frac{\partial\mathbf{B}}{\partial t} = \nabla\times(\mathbf{v}\times\mathbf{B}) - \nabla\times\mathbf{E}', \tag{2.5}$$

where $\mathbf{E}'$ is given by

$$E'_r = \frac{\eta}{r\sin\theta}\left[\frac{\partial}{\partial\theta}(B_\phi\sin\theta) - \frac{\partial B_\theta}{\partial\phi}\right],$$

$$E'_\theta = \frac{\eta}{r\sin\theta}\frac{\partial B_r}{\partial\phi},$$

$$E'_\phi = -\frac{\eta}{r}\frac{\partial B_r}{\partial\theta},$$

with $\eta$=$1/\mu\sigma$ the magnetic diffusivity (van Ballegooijen, Cartledge & Priest 1998). This assumes that there is no radial transport of the magnetic field, and that the meridional flow is poleward and the same as the solar value given by

$$u(\lambda) = \begin{cases} -u_0\sin(\frac{\pi\lambda}{\lambda_0}) & \text{if } |\lambda| < \lambda_0 \\ 0 & \text{otherwise} \end{cases} \tag{2.6}$$

where $\lambda \equiv \frac{\pi}{2} - \theta$ is the latitude, $\lambda_0$ gives the latitude above which the meridional flow is zero, $\lambda_0 = 75°$ and $u_0 = 11\text{m s}^{-1}$ which is close to the predicted value (Kitchatinov & Rüdiger 1999). The values of $B_{lm}$,$A_{lm}$ and $J_{lm}$ are evolved using the induction equation according to the meridional flow, the observed differential rotation and using various values of the magnetic diffusion, ranging from 250 to 550 $\text{km}^2\text{s}^{-1}$ (*cf.* the solar value of 450 $\text{km}^2\text{s}^{-1}$).

The differential rotation is of the form

$$\Omega(\theta) = 12.2434 - 0.0564\cos^2\theta \text{ rad d}^{-1} \tag{2.7}$$

where $\Omega$ is the rotation rate (Donati & Collier Cameron 1997). We have assumed that $\eta$ is uniform across the surface, although there is evidence that this may not be the case for the Sun (Berger et al. 1998).

## 2.3 Calculating the evolved field

The third stage is to take the evolved coefficients $B_{lm}$,$A_{lm}$ and $J_{lm}$ and the associated Legendre functions $P_{lm}$ and calculate the three components of the magnetic field- $B_r$ (radial), $B_\phi$ (azimuthal) and $B_\theta$ (meridional)- from them. These will be given by

$$B_r(r,\theta,\phi) = \sum_{l=1}^{N} \sum_{m=-l}^{l} B_{lm} P_{lm}(\theta) e^{im\phi}$$

$$B_\theta(r,\theta,\phi) = -\sum_{l=1}^{N} \sum_{m=-l}^{l} \lambda_l \left[ -A_{lm}(r) \frac{dP_{lm}}{d\theta} + iJ_{lm} \frac{mP_{lm}}{\sin\theta} \right] e^{im\phi}$$

$$B_\phi(r,\theta,\phi) = -\sum_{l=1}^{N} \sum_{m=-l}^{l} \lambda_l \left[ -A_{lm}(r) \frac{imP_{lm}}{\sin\theta} - J_{lm} \frac{dP_{lm}}{d\theta} \right] ime^{im\phi}$$

where

$$\lambda_l = \frac{1}{l(l+1)}$$

## 2.4 ZDI and calculating $\alpha$

One problem with Zeeman Doppler imaging from circularly polarised data is that it is not very sensitive to low latitude meridional field features (Donati & Brown 1997). In order to determine $\alpha$ however, we need to know how the meridional field $B_\theta$ varies with azimuth. Our solution to this was to calculate the potential field from the $B_r$ component (see next section) and to use the calculated value of $B_\theta$ from that, but to still use the observed $B_r$ and $B_\phi$ components. We have also investigated the alternative approach, which is to calculate $\alpha$ assuming $B_\theta = 0$. The distributions of $\alpha$ values are qualitatively unchanged although the numerical values of $\alpha$ are different.

We calculated the distribution of $\alpha$ from the observations. For each data set we constructed histograms of the values of $\alpha$. In Fig 2.1, the solid line represents $\alpha$ calculated assuming that $B_\theta = 0$ and the dotted line represents $\alpha$ calculated on the assumption that $B_\theta$ is given by the potential approximation. We have only plotted $-20 \leq \alpha \leq 20$. This shows that, with either assumption about $B_\theta$ the distributions of $\alpha$ determined from the observations are symmetric and centred on zero. If the stellar magnetic field were potential we would expect $\alpha$ to be zero everywhere, but

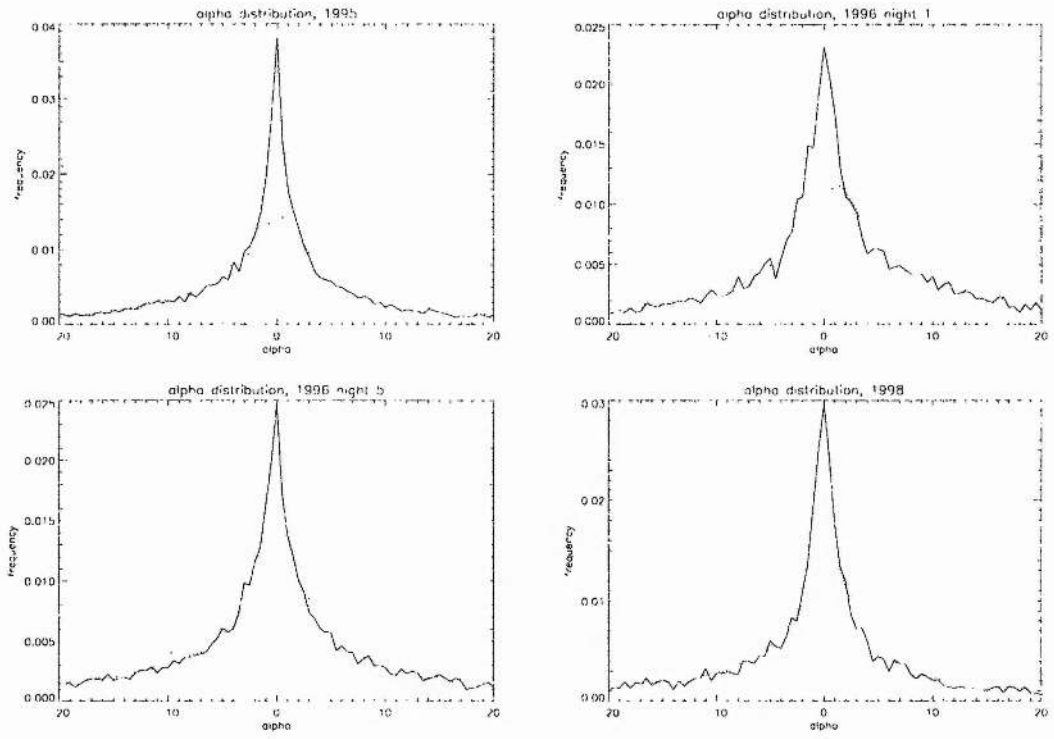


Figure 2.1: The frequency distribution of values of $\alpha$ between -20 and 20 for the observed fields for 1995 (top left), 23/25 Dec 1996 (top right), 29 Dec 1996 (bottom left) and 1998 (bottom right). $\alpha$ is calculated for latitudes between the equator and 80°north. The solid line is for the case where we assumed $B_\theta = 0$ and the dotted line for the case where we assumed $B_\theta$ was given by the potential approximation. $\alpha$ is in units of $10^{-8}\mathrm{m}^{-1}$. The binsize in these units is $\frac{1}{2}$.

- we do not have infinite resolution in the observations- for example, the 1996 observations have a spatial resolution of about 2°.9 at the equator (Donati et al. 1999),
- we do not have infinite resolution in the calculations since the values are calculated on a numerical grid and
- we have to truncate the Fourier series used in calculating the components of the field (see next section).

We can see that when new flux is created, there is no overall preference for the sign of $\alpha$.

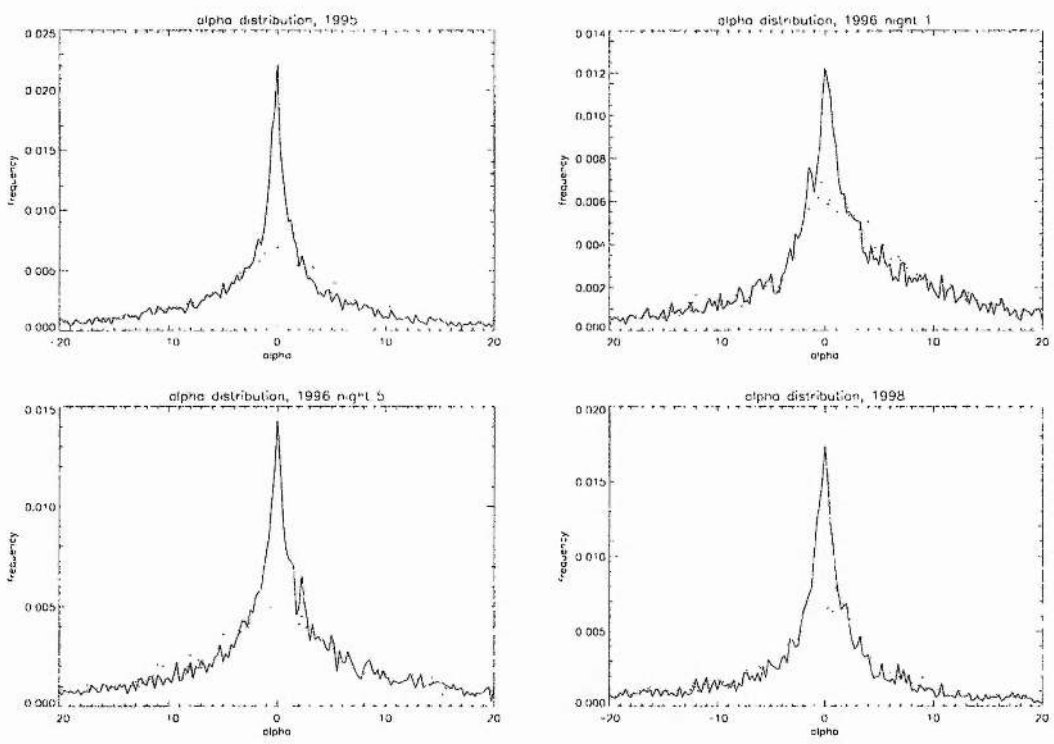


Figure 2.2: The frequency distribution of values of $\alpha$ between -20 and 20 for the observed fields for 1995 (top left), 23/25 Dec 1996 (top right), 29 Dec 1996 (bottom left) and 1998 (bottom right). $\alpha$ is calculated for latitudes between the equator and 60°north. The solid line is for the case where we assumed $B_\theta = 0$ and the dotted line for the case where we assumed $B_\theta$ was given by the potential approximation. The units and binsize are the same as in figure 2.1.

## 2.5 Temporal evolution of the magnetic field

Having satisfied ourselves that the use of a potential field is reasonable as a starting point for studying the magnetic field of AB Doradûs, we may proceed to study how that field would evolve subject to the observed differential rotation, the meridional flow and the effects of diffusion.

We are using a code originally developed by van Ballegooijen, Cartledge & Priest (1998) to study the formation of filament channels on the Sun. It can also be used to study the field of AB Doradûs because we have high-resolution magnetic maps (2?9 at the equator) and the differential rotation is similar to the solar value. The code takes the observed surface radial component of the field and calculates a potential field from this, and then evolves the calculated magnetic field due to the effects of differential rotation and diffusion.

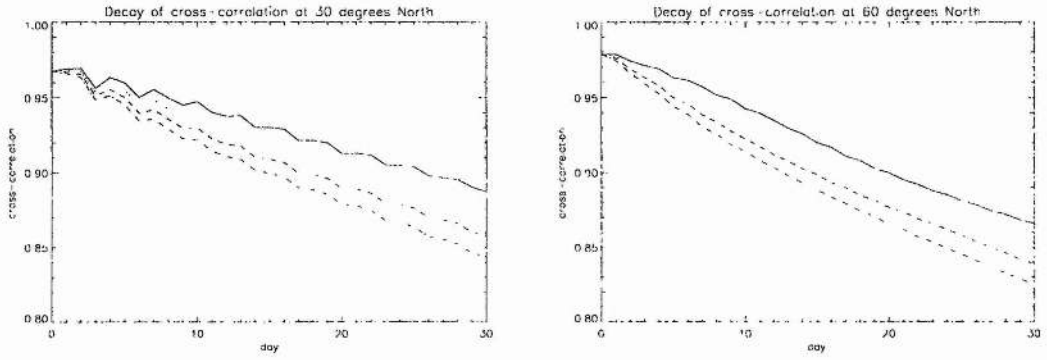


Figure 2.3: Cross-correlation of calculated radial field with the observed radial field for 1995, latitude 30°(left) and 60°(right). The solid line represents $\eta = 250\text{km}^2\text{s}^{-1}$, the dotted line $\eta = 350\text{km}^2\text{s}^{-1}$, the dashed line $\eta = 450\text{km}^2\text{s}^{-1}$ and the dot-dash line $\eta = 550\text{km}^2\text{s}^{-1}$. We should not expect a cross-correlation of exactly 1 at day 0 since we are correlating an observed field with a calculated one.

## 2.6 Cross-correlation of the observed and calculated radial fields

We took the observed field for the 1995 and 1998 observations and evolved it over 30 days according to the induction equation 2.5. This allowed us to study the variation with time of the cross-correlation of the radial component observed on the first night with that calculated for subsequent nights (Fig 2.3). We chose two latitudes: 30 and 60°north. The results for 1998 are qualitatively similar. In all cases, the cross-correlation function decays by approximately 10% over 30 days. Although choosing a higher value for the diffusivity does cause a more rapid decay of the field and hence a faster decay of the cross-correlation function, it is still not enough to explain the complete lack of correlation found by Barnes et al. (1998) for He699, a young G-dwarf in the $\alpha$ Persei cluster. It appears that for AB Doradûs, if diffusion and differential rotation were the only processes causing the field to evolve, that even after one month there should still be a good correlation.

## 2.7 Magnetic energy

We also looked at how the magnetic energy in the field at the surface evolved, calculating the ratio of magnetic energy in the evolved case to the original.

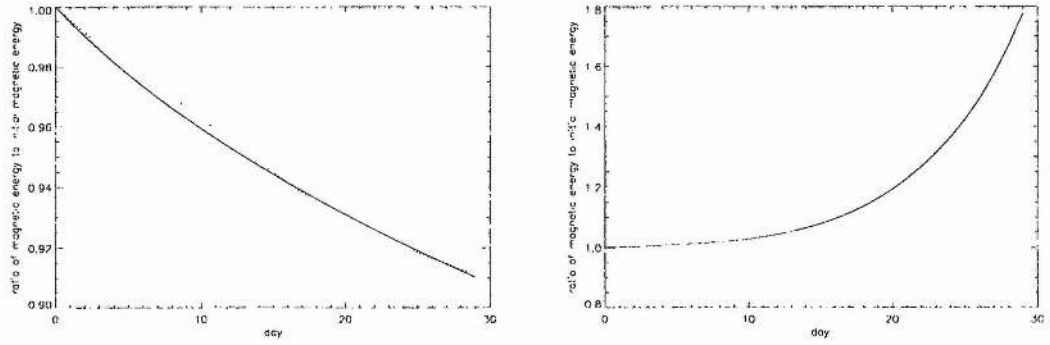


Figure 2.4: This shows how the magnetic energy varies as the field evolves for 1998. The left hand diagram is for the case when $\eta$=250km$^2$s$^{-1}$, with differential rotation (solid line) and without (dotted line), and the right hand diagram compares the case where there is no diffusion, i.e. $\eta = 0$ (solid line) and where $\eta$=250km$^2$s$^{-1}$ (dotted line)

A magnetic field has energy $B^2/2\mu$ per unit volume, so the total energy is

$$W = \int_{volume} \frac{B^2}{2\mu} dV$$

Fig 2.4 shows this for the 1998 field. We see that with no diffusion the magnetic energy increases, whereas with diffusion the magnetic energy decreases.

## 2.8 Evolution of $\alpha$

Another question is how the distribution of $\alpha$ should vary with time. For this we examined the 1995 data, taking the observed radial field and evolving it for 5,10,20 and 30 days. Examining the case where $\eta$=450km$^2$s$^{-1}$, we found that the peak of the frequency of values of $\alpha$ slowly shifted to the positive values while also decreasing in strength so that after being evolved for 30 days there was no discernable peak (Fig 2.5). We found qualitatively similar results for the other diffusion values considered.

Once again, our simple evolution of the field has produced a result that is in conflict with the observational evidence. As shown in Fig 2.1, the distribution of $\alpha$-values is observed to be symmetric about zero. From our model, however, the shearing effect of the differential rotation should produce a distribution of $\alpha$-values that is predominately positive. This conflict can be resolved, however, if we allow new flux to emerge through the surface and change the

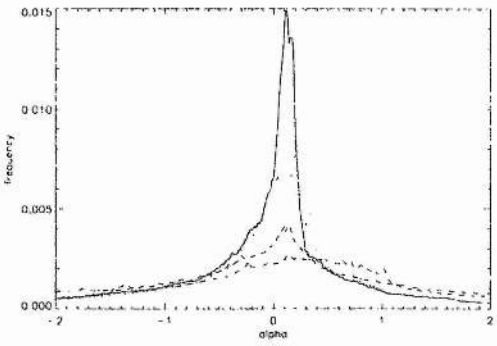


Figure 2.5: The frequency distribution of $\alpha$ between -2 and 2 for the evolved 1995 data with $\eta$=450km$^2$s$^{-1}$. The solid line represents day 5, the dotted line day 10, the dashed line day 20 and the dot-dash line day 30. Here the binsize is 0.01. $\alpha$ is in units of $10^{-8}$m$^{-1}$.

field distribution on a more rapid timescale than differential rotation or diffusion can act.

## 2.9 Evolution on a shorter timescale: comparison with observations

For 1996 we had two sets of magnetic maps, separated by 5 nights, and because of this our analysis was slightly different from that for the 1995 and 1998 data sets.

We have evolved the 23/25 Dec 1996 field using various values of the diffusion coefficient and compared that with the observed radial field for 29 Dec 1996. Using these, we were able to cross-correlate the calculated radial field for various values of the diffusion coefficient with the observed radial field for 29 Dec (Fig 2.7). We also considered the case where there was no differential rotation, enabling us to study the effect of differential rotation on the evolution of the field (Fig 2.8).

We ensured that the cross-correlation only involved those longitudes that were observed, *viz.* 18-180° (Jardine et al. 1999), and latitudes between 0 and 80° North. For each latitude, the cross-correlation was performed for various shifts in longitude, and the maximum value for each latitude calculated.

From these we see that altering the value of the diffusion and removing the differential rotation have little effect on the cross-correlation over 5 nights. We would need observations over a longer timescale, say a month, to be able to look for meaningful results. Because of this,

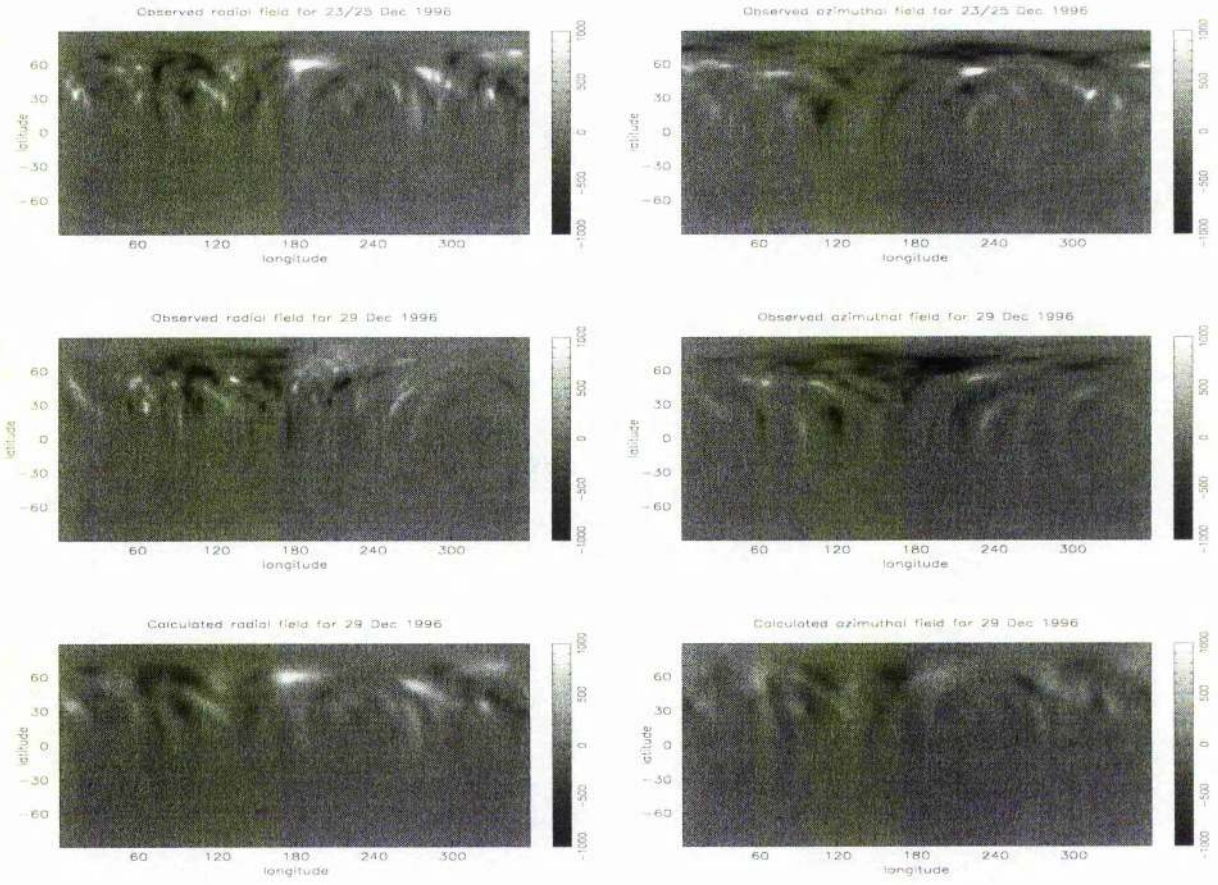


Figure 2.6: This diagram shows the azimuthal and radial components of the field in 1996. The top row gives the observed radial (left) and azimuthal (right) fields for 23/25 Dec. The middle row gives the observed radial (left) and azimuthal (right) fields for 29 Dec. The bottom row gives the calculated radial (left) and azimuthal (right) fields for 29 Dec, assuming that $\eta$=450km$^2$s$^{-1}$.

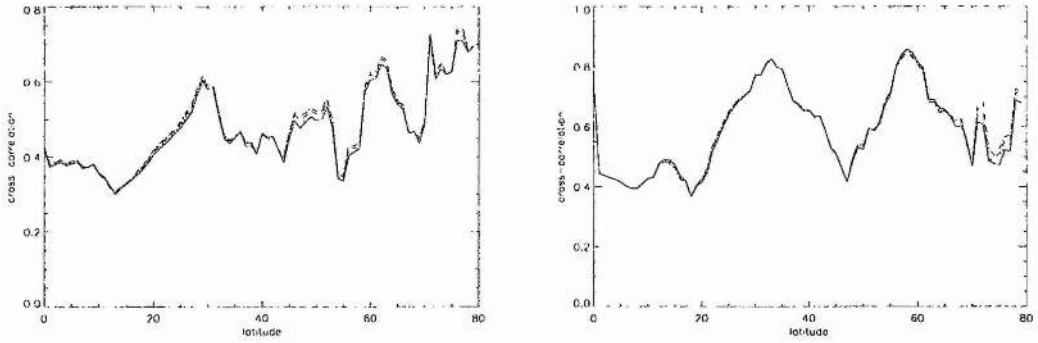


Figure 2.7: The peak amplitude of the cross-correlation function between the observed and calculated radial (left) and azimuthal (right) fields for latitudes between 0 and 80°north for 29 Dec 1996. The solid line represents $\eta = 250\text{km}^2\text{s}^{-1}$, the dotted line $\eta = 350\text{km}^2\text{s}^{-1}$, the dashed line $\eta = 450\text{km}^2\text{s}^{-1}$ and the dot-dash line $\eta = 550\text{km}^2\text{s}^{-1}$

we decided only to include the fields calculated with the observed differential rotation and with $\eta$=450km$^2$s$^{-1}$. The others are similar.

Figure 2.6 shows the observed radial and azimuthal fields for 23/25 Dec (top), the observed fields for 29 Dec (middle) and the calculated fields for 29 Dec (bottom), calculated on the assumption that $\eta$=450km$^2$s$^{-1}$.

## 2.10 The effect of the differential rotation

Jardine et al. (1999) demonstrated that the high-latitude azimuthal band of field was not reproduced by modelling the field as a potential one. The question we addressed was whether the differential rotation could produce this band.

To investigate this we took the 1998 field, evolving it for 5 days, and comparing the mean value of $B_\phi$ latitude by latitude. We decided to, at the same time, investigate the effect of imposing a uniform polar cap on the observed radial field.

From Doppler imaging of the RS Canum Venatorium type variable, HR 1099, Vogt & Penrod (1983) suggested that it had a polar spot.

We decided that the cap would extend down to 80° . The values tested for the cap were

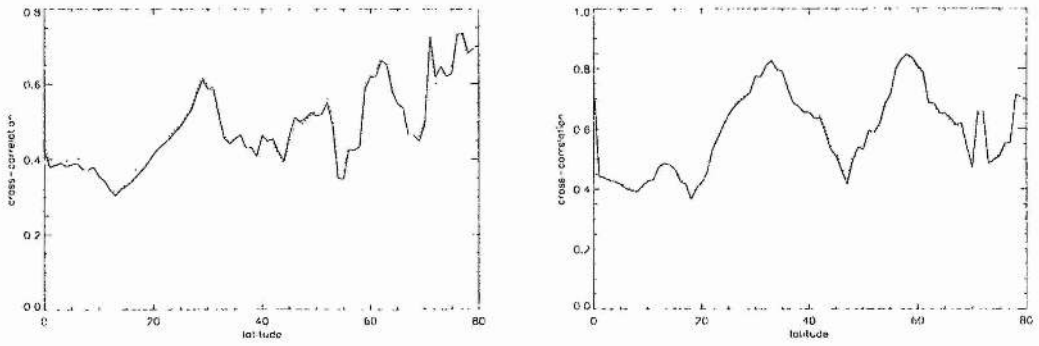

Figure 2.8: The peak amplitude of the cross-correlation function between the observed and calculated radial (left) and azimuthal (right) fields for latitudes between 0 and 80°north for 29 Dec 1996 with $\eta = 450\text{km}^2\text{s}^{-1}$. The solid line is with the differential rotation, and the dotted line is without the differential rotation

0G, ±1000G and ±4000G (*cf* a polar field strength of ∼1-2G for the sun (Babcock & Babcock 1955)).

We see that a high-latitude azimuthal band of negative polarity is produced when we use the observed differential rotation, and a high-latitude band of positive polarity is produced by using the reverse differential rotation. This indicates that the observed differential rotation is capable of producing a high-latitude negative azimuthal band.

The position of this peak in the observed field is remarkably similar for the different data sets. However, the mean values of $B_\phi$ for the unevolved potential fields are much smaller. As Fig 2.6 shows for the 1996 data, the potential case does produce plenty of structure in the distribution of $B_\phi$ at high latitudes. These two facts can be reconciled since the positive and negative values of $B_\phi$ at high latitude in the potential case almost cancel each other out.

We see from Fig 2.10 that when the 1998 observations were evolved for 5 nights the mean values of $B_\phi$ were negative for each northen latitude. We tried various values of the polar cap and, as Fig 2.9 shows, we needed a negative polar cap for the mean of $B_\phi$ to be negative at high northern latitudes.

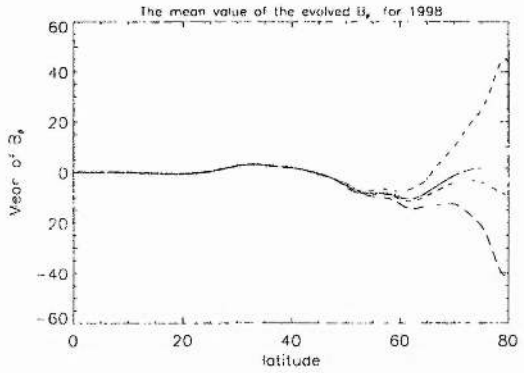


Figure 2.9: This shows the calculated values of the mean of $B_\phi$ latitude-by-latitude, from the 1998 data, evolved for 5 nights with $\eta = 250\text{km}^2\text{s}^{-1}$ and with different values of the polar cap. The solid line is the case where the polar cap is set to 0G, the dotted line where it is set to +1000G, the dashed line where it is set to -1000G, the dash-dot line where it is set to +4000G and the long-dashed line where it is set to -4000G

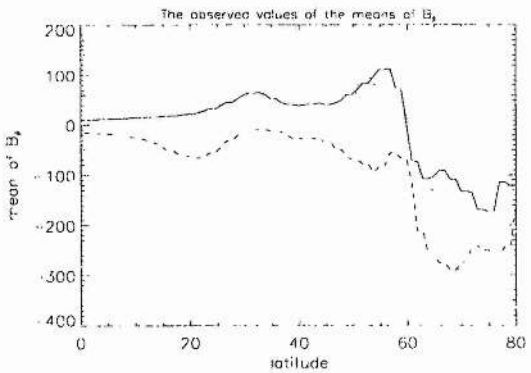


Figure 2.10: This shows the mean values of $B_\phi$ latitude-by-latitude for the observed field for 1995 (solid line), 1996 Dec 23/25 (dotted line) and 1998 (dashed line)

## 2.11 Conclusion

We have modelled the evolution of the magnetic field of AB Doradûs due to the effects of differential rotation and diffusion. We use as a starting point the Zeeman Doppler images obtained on three consecutive years and assume that the field is initially potential, but evolves away from this state as a function of time. This evolution is characterised by a drift in the distribution of the values of $\alpha$ (where for a force-free field $\nabla \times \mathbf{B} = \alpha \mathbf{B}$). We have shown that the distribution of $\alpha$-values calculated from the observed surface magnetic maps is symmetric and centred on zero, as is the case for the distribution obtained for our (model) potential field.

It takes some 20 to 30 days for the distribution of $\alpha$-values from our evolved magnetic fields to depart significantly from that for a potential field. Over this timescale we have determined, as a function of time, the cross-correlation of our model radial magnetic field with the observed radial component on the first night. We find that over one month, the cross-correlation function decays by about 10%. Observations of He699 by Barnes et al. (1998) show however that cross-correlating the observed spot distributions over this timescale gives much more rapid decrease of the cross-correlation function. Both this result and the fact that the evolution of the distribution of $\alpha$-values for our model magnetic fields is quite different to that observed suggest that the evolution of AB Doradûs's surface magnetic field is not governed solely by diffusion and differential rotation. We conclude that these results are more likely to be due to the effects of flux emergence changing the spot distribution than the effects of diffusion or differential rotation.

This result is independent of the assumed degree of field diffusion. We have compared the effects of values of $\eta$ ranging from 250 to 450 $\mathrm{km^2 s^{-1}}$ and found the results to be qualitatively the same. The presence of some diffusion is of course necessary (and we have confirmed that the magnetic energy grows monotonically with time in the absence of diffusion). The exact value of $\eta$ seems however to have little effect.

Since diffusion has little effect on the flux distribution, the differential rotation acts simply to advect the field. Consequently, although at each latitude the peak of the cross-correlation function may be at a different longitude Donati & Collier Cameron (1997), its actual value is virtually unchanged by the effects of differential rotation.

We have also compared the radial and azimuthal magnetic fields generated by our model

over 5 nights with those obtained from Zeeman Doppler images on 23/25 Dec and 29 Dec 1996 and found the agreement to be excellent. The evolution of the azimuthal field is of particular interest because the presence of the band of high latitude unidirectional azimuthal field in the observed maps.

By studying the position of the field lines originating in the north polar cap, we found that these lines mainly end at high northern latitudes. The direction of these field lines depends strongly upon the distribution of radial field at mid to high latitudes. Changing the strength of the polar cap has little effect on field lines at low latitude. This corresponds to our result that $\sum B_\phi$ varies little at low latitude as the strength of the cap is altered (as seen in Fig 2.9).

We have investigated whether the shearing effect of the differential rotation is sufficient to generate this band of field. The strength of this band depends upon the strength and sign of the radial field in the polar cap. A negative cap creates a stronger high latitude band than a positive cap does.

While we cannot reproduce a high latitude azimuthal band of the same strength as is observed, our results suggest that the differential rotation plays a major part in the creation and preservation of the high latitude azimuthal band.

CHAPTER 3

# Prominences

## 3.1 Introduction

Robinson & Collier Cameron (1986) observed four H$\alpha$ transient features in the spectrum of AB Doradûs in December 1984, and– from the rapid drift rates– suggested they could be caused by large clouds of absorbing material, which would be high above the surface (the mean value was 2.5 $R_*$ and about 1.25 $R_*$ above the equatorial plane) and co-rotating with the star. They suggested one of the features was as far as 4 $R_*$ above the surface.

They argued that if this was the case, these are being forced to co–rotate by an ambient magnetic field, showing that magnetic fields exist high in the corona.

Any model of stability would have to explain how prominences can be stable at large distances from the star and high above the equatorial plane.

Collier Cameron & Robinson (1989a) investigated the H$\alpha$ spectra of AB Doradûs from observations taken in December 1984 and January 1986, finding little evidence for the deep H$\alpha$ absorption features expected from early K dwarfs. The profile was filled to nearly the continuum level, which they suggested was due to chromospheric emission from plage-like activity widespread on the stellar surface.

They found the absorption features to be narrow, with a FWHM ranging between 1.0 and 2.9 Å.

They studied the evolution of the radial velocity (RV) of the absorption features, noticing:

1. The RV drifts approximately linearly blueward to redward,
2. At the bluest RV, the equivalent width (EW) is small and rapidly increasing,
3. as the RV moves redward, the blue wing remains stationary, with the red wing moving to redder wavelengths and the profile deepening,
4. eventually, the EW stops increasing, and the blue and red wings drift redward at the same rate,
5. the red wing remains stationary, with the EW decreasing and the blue wing drifting redward.

They argued that the small FWHM of the H$\alpha$ absorption features and the drift from blue to red indicated rotational modulation, but were able to rule out features on the stellar surface, as a surface feature would cross the disc in approximately 6 hours, whereas the absorption transients take about 1-2 hours to cross. They suggested that the absorption transients could be due to clouds of cool, dense gas, in corotation with AB Doradûs. They show that if this is the case, then it provides evidence of closed magnetic loops larger than those on the Sun.

Collier Cameron & Robinson (1989b) used November 1986 observations of AB Doradûs to investigate the evolution of these clouds over an interval of a few nights.

They found that the clouds are forming near the corotation radius on a timescale of 1-2 days, and so, to keep the number of clouds reasonably constant, they must be destroyed and/or ejected on a similar timescale.

They found that clouds were being ejected at speeds $\sim$20 km s$^{-1}$, with the speed increasing as the distance increased. The acceleration was much smaller than that which would be expected if they were moving freely along open, radial fieldlines corotating with AB Doradûs. This indicates that the confining magnetic field is still in existence at distances of 9R$_*$.

Collier Cameron et al. (1990) used H$\alpha$, Ca II H & K and Mg II h & k in the optical and ultraviolet spectra of AB Doradûs to study the physical properties of the prominences- in particular, the column densities, temperatures and the turbulent internal motion.

They used that facts that the equivalent width of H$\alpha$ lines is sensitive to the column density and the temperature, rather than the internal motions, and the Ca II and Mg II are

more sensitive to the column density and the internal motions.

From the equivalent width of H$\alpha$ lines they showed that the temperature of the prominences are around 8000-9000K.

Donati et al. (1999) used observations of AB Doradûs from December 1996 and detected prominences between 2.5 and 4.7$R_*$ from the stellar rotation axis, seeing four prominences on more than one night.

## 3.2 Stability

For a prominence to be stable, two conditions need to be satisfied:

$$\mathbf{g}.\mathbf{B} = 0, \tag{3.1}$$

and

$$\mathbf{B}.\nabla(\mathbf{g}.\mathbf{B}) < 0. \tag{3.2}$$

Here $\mathbf{g}$ represents the *effective gravity*, which includes a centrifugal term as well as the gravitational term. Its components in spherical co-ordinates are:

$$g_r = -\frac{GM_*}{r^2} + \omega^2 r \sin^2\theta, \tag{3.3}$$

$$g_\theta = \frac{1}{2}\omega^2 r \sin 2\theta, \tag{3.4}$$

and

$$g_\phi = 0. \tag{3.5}$$

Equation 3.1 requires that the effective gravity and the magnetic field are perpendicular. In equation 3.2, the left–hand side is the directional derivative of $\mathbf{g}.\mathbf{B}$ along a magnetic field–line, i.e. a measure of the rate of change of $\mathbf{g}.\mathbf{B}$ along the field–line in question. If equation 3.2 holds, then $\mathbf{g}.\mathbf{B}$ is decreasing in the direction of $\mathbf{B}$.

The co-rotation radius (also called the Keplerian radius), $r_K$ is defined to be the radius in the equatorial plane where $\mathbf{g} = 0$, thus at a point in spherical co-ordinates $(r_K, \pi/2, \phi)$, the effective gravity would be zero. This radius is given by

$$r_K = \left(\frac{GM_*}{\omega^2}\right)^{1/3}. \tag{3.6}$$

For this work, I decided, for reasons of simplicity to use *Wilson-Devinney units*, for which $r_K = 1$ and all radii are scaled to this. If $r_{WD}$ is a distance in Wilson-Devinney units, then

$$r_{WD} = \frac{r}{r_K}, \tag{3.7}$$

which is equivalent to

$$r_{WD} = r\left(\frac{\omega^2}{GM_*}\right)^{1/3}. \tag{3.8}$$

With these units, the form of the effective gravity is simply

$$g_r = (\omega^4 GM_*)^{\frac{1}{3}}(r\sin^2\theta - \frac{1}{r^2}),$$

$$g_\theta = (\omega^4 GM_*)^{\frac{1}{3}}\frac{r}{2}\sin 2\theta,$$

and

$$g_\phi = 0.$$

It can be seen that in the equatorial plane ($\theta = 90°$), $\sin\theta = 1$. Hence

$$g_r \propto r - \frac{1}{r^2}.$$

Thus $g_r$ flips sign at the corotation radius.

$$g_r \begin{cases} < 0 & \text{if } r < 1, \\ > 0 & \text{if } r > 1, \\ = 0 & \text{if } r = 1. \end{cases}$$

Collier Cameron (1988) studied stability of large stellar loops. He showed that for large loops (extending beyond $r_K$) then at the summit the centrifugal term of $g_r$ dominates. Then hydrostatic equilibrium means that the pressure *increases* outwards along the loop beyond $r_K$. Thus the electron density $n_e$ must increase outwards in the outermost parts of such loops.

In a fully ionised plasma, the radiative loss function $L_r$ is related to $n_e$ by

$$L_r \propto n_e^2, \tag{3.9}$$

which may lead to thermal instability at the loop summit if the plasma is centrifugally compressed beyond corotation. However, he showed that normally the conduction dominates, ensuring thermal stability along the loop. From this he argued that large coronal loops are possible.

## 3.3 Dipole

The first case looked at was a dipole(*cf.* Ferreira 2000), given by

$$B_r = 2\frac{B_0}{r^3}\cos\theta, \tag{3.10}$$

$$B_\theta = \frac{B_0}{r^3}\sin\theta, \tag{3.11}$$

and

$$B_\phi = 0. \tag{3.12}$$

In Wilson-Devinney units these become

$$B_r = 2\frac{B_0\omega^2}{r^3 GM_*}\cos\theta,$$

$$B_\theta = \frac{B_0\omega^2}{r^3 GM_*}\sin\theta,$$

and

$$B_\phi = 0,$$

so that

$$\mathbf{g}.\mathbf{B} = \frac{B_0}{r^5}\left(\frac{\omega^5}{GM_*}\right)^{\frac{2}{3}}\cos\theta(3r^3\sin^2\theta - 2), \tag{3.13}$$

which means that $\mathbf{g}.\mathbf{B} = 0$ when

$$r = \left(\frac{2}{3\sin^2\theta}\right)^{\frac{1}{3}}. \tag{3.14}$$

There is an alternative solution when $\cos\theta = 0$, which occurs at the equator.

At each point $(r, \theta, \phi)$

$$\mathbf{B}.\nabla(\mathbf{g}.\mathbf{B}) = \frac{B_0^2}{r^9}\left(\frac{\omega^{16}}{(GM_*)^5}\right)^{\frac{1}{3}}\left[20 - 6r^3\sin^2\theta - 18\sin^2\theta + 3r^3\sin^4\theta\right]. \tag{3.15}$$

As

$$\frac{B_0^2}{r^9}\left(\frac{\omega^{16}}{(GM_*)^5}\right)^{\frac{1}{3}} > 0$$

we need only consider the sign of

$$20 - 6r^3\sin^2\theta - 18\sin^2\theta + 3r^4\sin^4\theta. \tag{3.16}$$

When the relationship between $r$ and $\theta$ is given by 3.14, then 3.16 is simply

$$16(1 - \sin^2\theta), \tag{3.17}$$

which is always greater than or equal to 0 for $\theta \in \Re$. Thus there are no stable points outside of the equatorial plane.

In the equatorial plane however, 3.15 reduces to

$$\mathbf{B}.\nabla(\mathbf{g}.\mathbf{B}) = \frac{B_0^2}{r^9}\left(\frac{\omega^{16}}{(GM_*)^5}\right)^{\frac{1}{3}}(2 - 3r^3), \tag{3.18}$$

which is less than 0 when

$$r > \left(\frac{2}{3}\right)^{\frac{1}{3}}. \tag{3.19}$$

For ease of notation, I will define $r_L$ to be

$$r_L = \left(\frac{2}{3}\right)^{\frac{1}{3}}, \tag{3.20}$$

which is the boundary between the cases where 3.19 is and isn't satisfied.

This gives $r_L \approx 0.8736$.

The stable surface for a dipole is shown in figures 3.1–3.3.

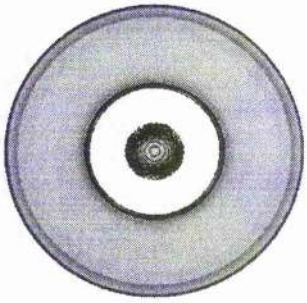

Figure 3.1: The stable surface for a dipole viewed pole-on. In this and the following two diagrams, the stable sheet extends to infinity– for plotting purposes there has been a cut–off at $\sim 5R_*$.

Figure 3.2: The stable surface for a dipole viewed from an angle of 60 °

Figure 3.3: The stable surface for a dipole viewed from the equator

## 3.4 Source surface quasidipole

As can be seen from equation 3.11, the $B_\theta$ component of a dipole remains non-zero at very large distances from the star, hence there is no distance at which the field is completely radial.

With this in mind, I investigated what I will term a *source surface quasidipole*. The $B_r$ component of a dipole at the stellar surface was used to determine a potential field, subject to the source surface requirements given by equation 2.4.

The components of the source surface quasidipole are

$$B_r = \frac{2B_0}{R_*^3} \frac{1 + 2(\frac{r_s}{r})^3}{1 + 2(\frac{r_s}{R_*})^3} \cos\theta, \tag{3.21}$$

$$B_\theta = \frac{2B_0}{R_*^3} \frac{(\frac{r_s}{r})^3 - 1}{1 + 2(\frac{r_s}{R_*})^3} \sin\theta \tag{3.22}$$

and

$$B_\phi = 0. \tag{3.23}$$

.

$B_0$ is not a magnetic field strength– it is given by

$$B_(0) = \frac{1}{2}\tilde{B}_r R_*^3,$$

where $\tilde{B}_r$ is the radial magnetic field at the north pole on the stellar surface.

At the stellar surface

$$B_r = \frac{2B_0}{R_*^3}\cos\theta$$

and

$$B_\phi = 0,$$

just as they are for the dipole. However,

$$B_\theta = \frac{2B_0}{R_*^3}\frac{(\frac{r_s}{R_*})^3 - 1}{1 + 2(\frac{r_s}{R_*})^3}\sin\theta,$$

which is different to the value of $B_\theta$ for a dipole (eqn. 3.11).

However, consider what happens to

$$\frac{(\frac{r_s}{R_*})^3 - 1}{1 + 2(\frac{r_s}{R_*})^3}$$

when the source surface radius tends towards infinity. Both the numerator and the denominator tend to infinity. To get round this, and to avoid having to invoke L'Hôpital's rule, it is possible to divide both the numerator and denominator by $(\frac{r_s}{R_*})^3$, giving

$$\frac{1 - (\frac{R_*}{r_s})^3}{2 + (\frac{R_*}{r_s})^3}.$$

Then this fraction tends to $\frac{1}{2}$ as $r_s \to \infty$.

Thus, as $r_s \to \infty$,

$$B_\theta \to \frac{B_0}{R_*^3}\sin\theta,$$

which is the value for a dipole.

When $r = r_s$ then

$$B_r = \frac{3}{1 + 2(\frac{r_s}{R_*})^3}\cos\theta$$

and $B_\theta = B_\phi = 0$, giving a radial field at the source surface.

In Wilson-Devinney units

$$B_r = \frac{2B_0\omega^2}{GM_*R_*^3}\frac{1 + 2(\frac{r_s}{r})^3}{1 + 2(\frac{r_s}{R_*})^3}\cos\theta, \tag{3.24}$$

and

$$B_\theta = \frac{2B_0\omega^2}{GM_*R_*^3}\frac{(\frac{r_s}{r})^3 - 1}{1 + 2(\frac{r_s}{R_*})^3}\sin\theta. \tag{3.25}$$

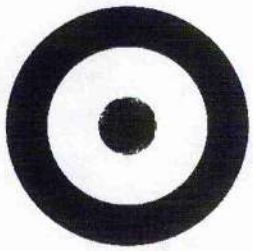

Figure 3.4: The stable surface for a quadrupole viewed pole-on

## 3.5 Quadrupole

For a quadrupole, the magnetic field components are given by

$$B_r = \frac{B_0}{r^4}(2 - 3\sin^2\theta),$$

$$B_\theta = \frac{B_0}{r^4}\sin 2\theta$$

and

$$B_\phi = 0,$$

which in Wilson-Devinney units are

$$B_r = \frac{B_0}{r^4}\left(\frac{\omega^2}{GM_*}\right)^{\frac{4}{3}}(2 - 3\sin^2\theta),$$

$$B_\theta = \frac{B_0}{r^4}\left(\frac{\omega^2}{GM_*}\right)^{\frac{4}{3}}\sin 2\theta$$

and

$$B_\phi = 0.$$

This gives us

$$\mathbf{g}.\mathbf{B} = B_0\frac{\omega^4}{GM_*}\left[\frac{\sin^2\theta}{r^3}[4 - 5\sin^2\theta] + \frac{1}{r^6}[3\sin^2\theta - 2]\right], \tag{3.26}$$

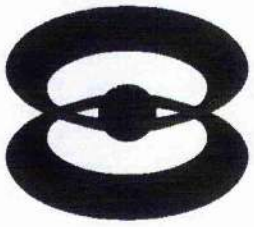

Figure 3.5: The stable surface for a quadrupole viewed from an angle of 60 °

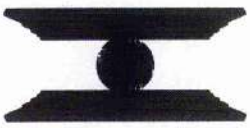

Figure 3.6: The stable surface for a quadrupole viewed from the equator

which has a solution

$$r^3 = \frac{3\sin^2\theta - 2}{\sin^2\theta(5\sin^2\theta - 4)} \tag{3.27}$$

Thus, for 3.2 to hold, we need

$$2(21\sin^4\theta - 30\sin^2\theta + 12) - r^3\sin^2\theta(5\sin^4\theta - 10\sin^2\theta + 8) < 0 \tag{3.28}$$

The only latitudes where this holds (when the relationship between $r$ and $\theta$ is given by equation 3.27) is between latitudes 16.61°and 26.56° (both north and south). For latitude 16.61°, from equation 3.27 it can be seen that $r \approx 1.116$ in Wilson–Devinney units, equivalent to $2.9R_*$ . $r$ increases as the latitude increases, tending asymptotically to infinity as the latitude approaches 26.56°.

## 3.6 Calculating the stable sheets

The stable sheets are numerically calculated for plotting in a several stage process.

1. The first step is to calculate $\mathbf{g}.\mathbf{B}$ in the region out to the source surface. This can be simply calculated as $B_r g_r + B_\theta g_\theta$, taking advantage of the fact that $g_\phi = 0$.
2. The angle, $\gamma$, between $\mathbf{g}$ and $\mathbf{B}$ is calculated from the definition of the scalar product, hence
$$|\cos\gamma| = \frac{|\mathbf{g}.\mathbf{B}|}{|\mathbf{g}||\mathbf{B}|}.$$
3. If $|\cos\gamma| < \frac{1}{20}$ then $\frac{\partial}{\partial r}\mathbf{g}.\mathbf{B}$ and $\frac{\partial}{\partial\theta}\mathbf{g}.\mathbf{B}$ are calculated nuerically from the values of $\mathbf{g}.\mathbf{B}$ at neighbouring points. This gives $\mathbf{B}.\nabla(\mathbf{g}.\mathbf{B})$.
4. A value, $v$, is assigned to each point
$$v = \begin{cases} -1 & \text{if } \mathbf{B}.\nabla(\mathbf{g}.\mathbf{B}) < 0, \\ 0 & \text{otherwise.} \end{cases}$$
5. The values of $v$ are then interpolated onto a cartesian grid.
6. The stable sheets are then plotted– a point with $v < v_{max}$ is plotted as stable. For each point $-1 \leq v \leq 0$.

Figure 3.7: The stable surface for 1996 night 1, viewed from the pole.

## 3.7 Stable sheets derived from the observations

Having seen how this technique can be used for calculating and plotting the stable sheets determined for the dipole, quasidipole and quadrupole, the next step is to calculate and plot the stable sheets for fields derived from the observations.

The aim of this is to see where prominences can exist and be stable.

For the 1996 night 1 data, figures 3.7–3.12 (and especially figures 3.8 and 3.12) show that the stable surface outside $r_L$ is concentrated in a highly–inclined feature on one side of the star and that inside $r_L$ is predominatly at a high northern latitude, although there is part of it at a high southern attitude. Figures 3.9 and 3.10 enable the stable sheets to be viewed at the same angle as AB Doradûs is inclined, so showing stable points passing in front of, above or below the star as viewed from Earth. Prominences passing in front of the stellar disc will be seen in absorption, and those which pass above or below the disc will be seen in emission.

The nearest stable points to AB Doradûs are at r=0.395 in Wilson-Devinney units. However, the stellar surface is at r=0.385. Thus these stable points are very close to the surface.

Figure 3.8: The stable surface for 1996 night 1, viewed from the pole. The left hand figure shows the surface inside $r_L$, and the right hand figure shows that outside.

Figure 3.9: The stable surface for 1996 night 1, viewed from 60°.

Figure 3.10: The stable surface for 1996 night 1, viewed from 60°. The left hand figure shows the surface inside $r_L$, and the right hand figure shows that outside.

Figure 3.11: The stable surface for 1996 night 1, viewed from the equator.

Figure 3.12: The stable surface for 1996 night 1, viewed from the equator. The left hand figure shows the surface inside $r_L$, and the right hand figure shows that outside.

CHAPTER 4

# Prominence positions and surface field topology

To study the effect of the surface field topology on the stable surfaces, it is necessary to trace the fieldlines passing through the stable surfaces back to their footpoints on the stellar surface. In this chapter, I investigated was the fieldlines through the stable points. What features on the surface were responsible?

## 4.1 Calculating the fieldlines

The equations for the fieldlines are:

$$\frac{dr}{B_r} = \frac{rd\theta}{B_\theta} = \frac{r\sin\theta d\phi}{B_\phi}. \tag{4.1}$$

(e.g. Priest 1984)

If $B_\phi = 0$ then equation (4.1) reduces to

$$\frac{dr}{d\theta} = r\frac{B_r}{B_\theta}, \tag{4.2}$$

which can be solved to give $r(\theta)$ for the fieldline.

## 4.2 Dipole

In the case of a dipole, the $B_r$ and $B_\theta$ components are given by equations (3.10) and (3.11), with $B_\phi = 0$. Hence equation (4.2) can be used and gives

$$\frac{dr}{d\theta} = 2r\cot\theta. \tag{4.3}$$

This can be separated into

$$\frac{dr}{r} = 2\frac{d\theta}{\tan\theta}, \tag{4.4}$$

which upon integrating, gives

$$\ln r = 2\ln\sin\theta + k, \tag{4.5}$$

where $k$ is some constant.

When $r = 1$ and $\theta = \theta_0$, then equation (4.5) gives

$$k = -2\ln\sin\theta_0, \tag{4.6}$$

hence

$$\ln r = 2\ln\left(\frac{\sin\theta}{\sin\theta_0}\right), \tag{4.7}$$

so the fieldline starting at a point $(\theta_0, \phi_0)$ on the surface can be described by

$$r = \left(\frac{\sin\theta}{\sin\theta_0}\right)^2 \tag{4.8}$$

and

$$\phi = \phi_0, \tag{4.9}$$

where $r$ is in units of stellar radius, and $\theta$ is the co-latitude. Such a fieldine is symmetric about the equator. The furthest distance the fieldline reaches from the star is

$$r = \csc^2\theta_0. \tag{4.10}$$

Some fieldlines are shown in figures 4.1 and 4.2.

## 4.3 The observations

The magnetic field is calculated from the observations by the method in chapter 2.

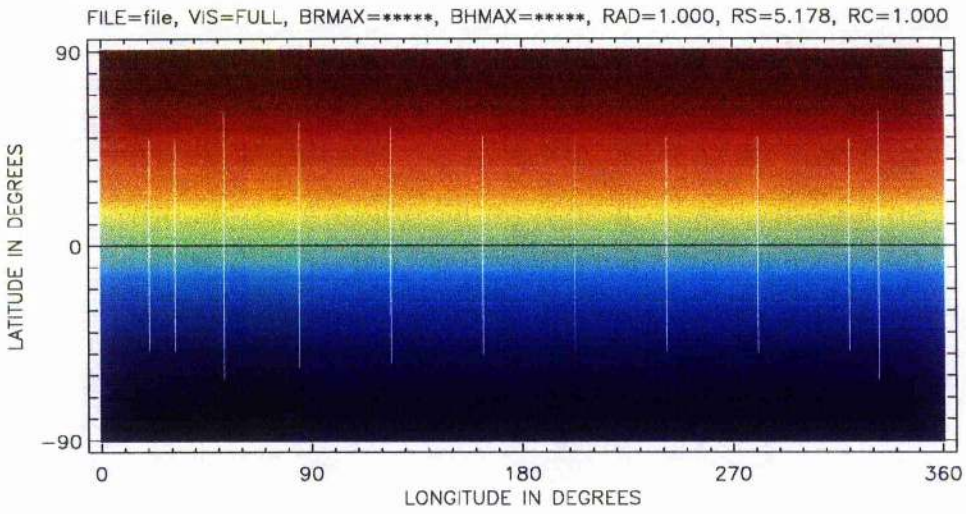


Figure 4.1: This shows the fieldlines for a dipole on a Cartesian grid

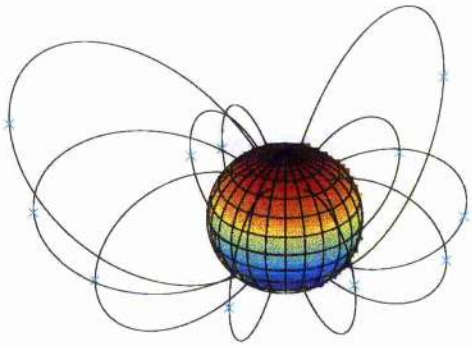

Figure 4.2: This shows the fieldlines for a dipole, viewed with the pole tilted 30° towards the observer. The crosses indicate the stable points.

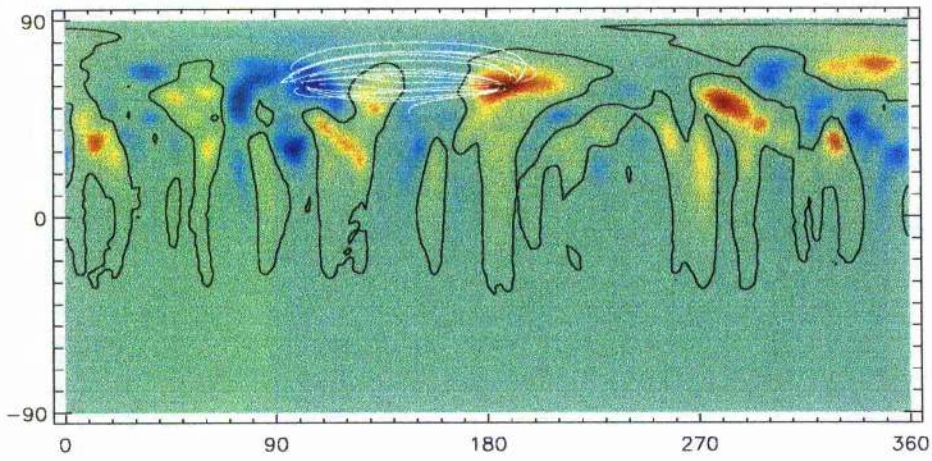


Figure 4.3: This shows the fieldlines for a stable surface at high northern latitudes for the 1996 night 1 data

### 4.3.1 A northern feature

The first stable surface I investigated was at high northern latitudes. The surface is shown in figure 4.4 and the fieldlines responsible for it in figure 4.3.

The fieldlines appear to be connecting a region of positive radial field at approximately (180–200,60–70), [where co–ordinates are given as (longitude,latitude)] with a region of negative field at approximately (100–120,60–70). As figure 2.6 shows, the former co–ordinates are linked with a strongly negative azimuthal field, whereas the azimuthal field at the latter co–ordinates is much weaker.

As can be seen from figure 4.4, much of this stable surface would always remain between the star and the observer, and any prominences would thus be seen in absorption.

### 4.3.2 A southern feature

The other major stable surface extended between longitudes 180–320°and from 20 to 40°south.

As figures 4.5 and 4.6 show, some of the fieldlines responsible for this stable surface

Figure 4.4: This shows a stable surface at high northern latitudes for the 1996 night 1 data, viewed at a longitude of 90°.

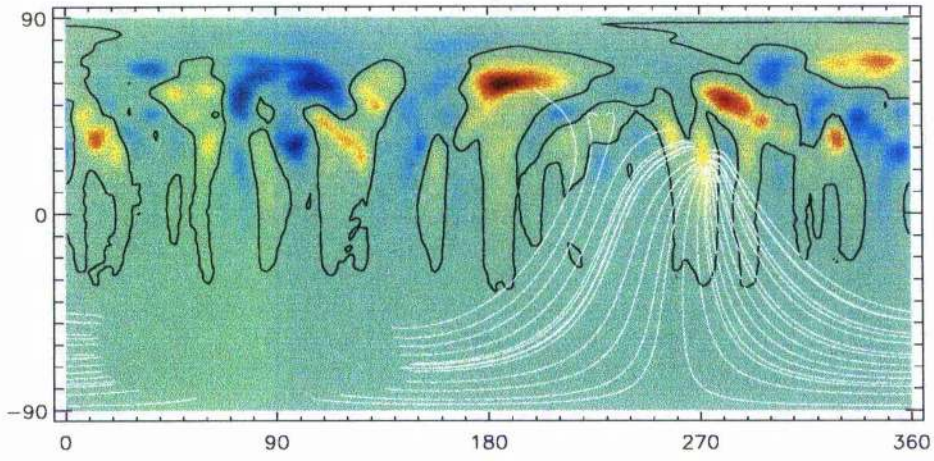


Figure 4.5: This shows the fieldlines for a stable surface at southern latitudes for the 1996 night 1 data

originate in the region of positive radial field at approximately (180–200,60–70), which was also responsible for the fieldlines at high northern latitude. The fieldlines terminated at points in the southern hemisphere which are too far south to be observed.

## 4.4 A combined field

One problem is that the field below $\sim$ -30° cannot be observed. This raises the question of whether field further south than that can affect the positions of observable prominences.

I assumed that the southern high–latitude field would be similar to the northern high–latitude field, and decided to investigate a combined field, given at the surface by

$$\mathbf{B}(R_*, \theta, \phi) = \mathbf{B_{96}}(R_*, \theta, \phi - 90^\circ) - \mathbf{B_{98}}(R_*, 180^\circ - \theta, \phi), \tag{4.11}$$

where $\mathbf{B_{96}}$ is the 1996 night 1 field and $\mathbf{B_{98}}$ is the 1998 field. The coronal field was then calculated by the technique in chapter 2. The 1996 night 1 field was rotated by 90° in longitude to reduce the possibility of the northern and southern hemispheres being nearly mirror–images of each other (as can be seen by comparing figure 1.3 with 1.4, some high–latitude features seem to appear in similar positions).

Figure 4.6: This shows a stable surface at southern latitudes for the 1996 night 1 data

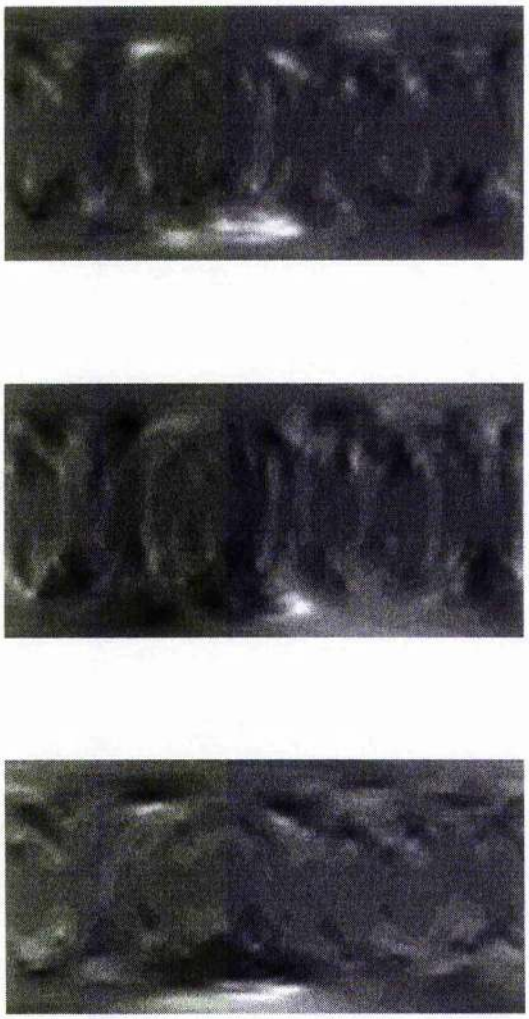

Figure 4.7: This shows the surface magnetic field derived by equation 4.11 from the 1996 and 1998 data. The top panel shows $B_r$, the middle panel $B_\phi$ and the bottom panel $B_\theta$.

Figure 4.8: This shows (LHS) the stable surface for the mixed field and (RHS) for the 1996 night 1 field, as viewed from the pole

The stable surfaces are shown in figures (4.8)–(4.10)

The first feature looked at was in figures (4.11) and (4.12), which is two stable surfaces in the southern hemisphere, at longitude $\sim 90°$. As figure (4.11) shows, this is caused by fieldlines from a region of strong positive radial field around (140–170,-50– -80), with the fieldlines terminating in a region of negative radial field around (50,-50). As can be seen from figure (4.12), it is possible for fieldlines from the same region of field on the stellar surface to cause distinct stable surfaces.

The stable surfaces would not transit the star.

One other possibility is a single stable surface being caused by several different features. Figures (4.13)–(4.16) give one such case.

The surface stretches from high northern to high southern latitudes, and lies between longitudes 265–290°. As figures (4.13) and (4.14) show, the far southern part of the surface is due to a region of strong positive radial field around (190,-60) with the fieldlines terminating around (320,-30).

The rest of the stable surface is due to fieldlines from several regions on the stellar surface, as figures (4.15) and (4.16) show.

Figure 4.9: This shows (LHS) the stable surface for the mixed field and (RHS) for the 1996 night 1 field, as viewed from 60°

Figure 4.10: This shows (LHS) the stable surface for the mixed field and (RHS) for the 1996 night 1 field, as viewed from the equator

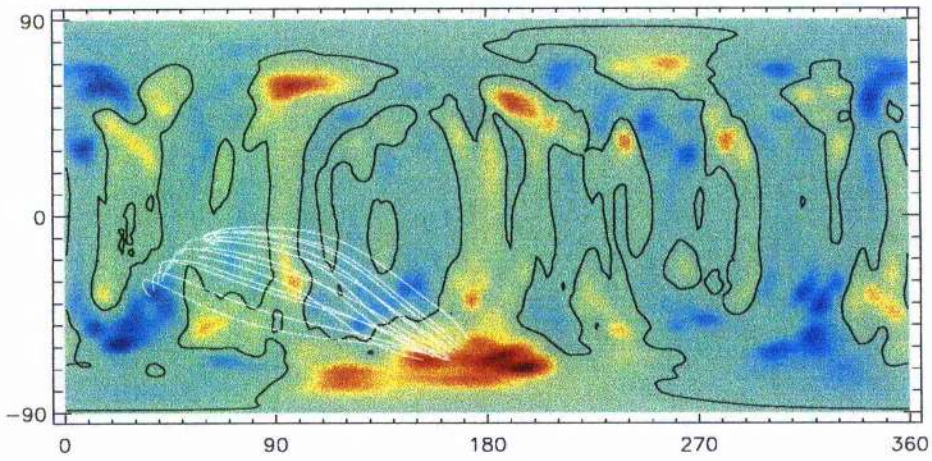


Figure 4.11: This shows the fieldlines causing two southern stable surfaces for the mixed field.

This surface will– in part– transit the star.

Creating a mixed field makes the stable surfaces more complicated, and has destroyed the semi–circular highly–inclined stable surface seen in figures (3.7)–(3.12). The possibility is also raised of transiting stable sheets caused by regions of surface magnetic field too far south to be observed. Careful observation of prominences which transit quickly (i.e. would transit the southern part of AB Doradûs) could provide hints to the surface magnetic field structure at high southern latitudes.

Donati et al. (2000) noted that the prominences for RXJ1508.6–4432 were forming between 1.3 and $2.0R_*$ (where the corotation radius was $1.65 \pm 0.10R_*$, leading to $r_L = 1.44 \pm 0.09R_*$), and tended to be confined to the equatorial plane– which they said was typical for ultra–fast rotators. Moreover, the prominences they observed were in emission, and not transiting the disc– hence the hypothesis that there are high–latitude prominences which are not seen because they do not cross the disc can be discarded.

Figure 4.12: This shows two southern stable surfaces for the mixed field, and the fieldlines responsible for them.

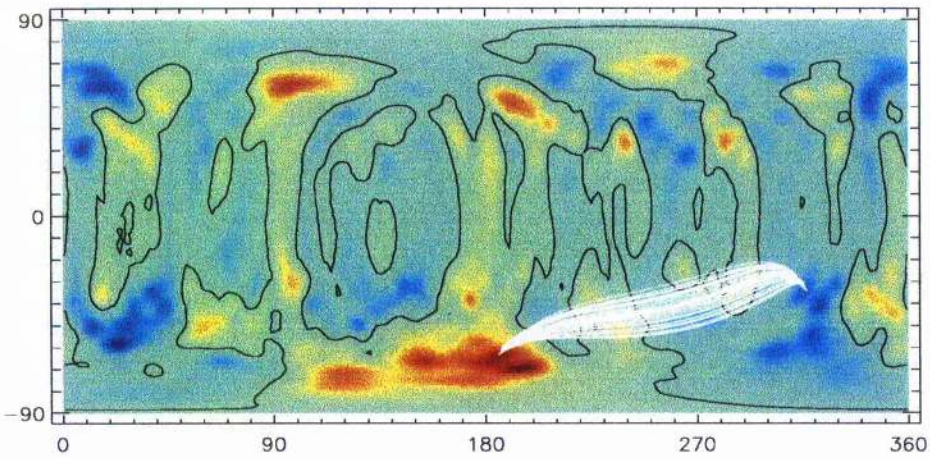


Figure 4.13: This shows the fieldlines responsible for the southern end of an stable surface for the mixed field

Figure 4.14: This shows the southern end of a stable surface for a mixed field

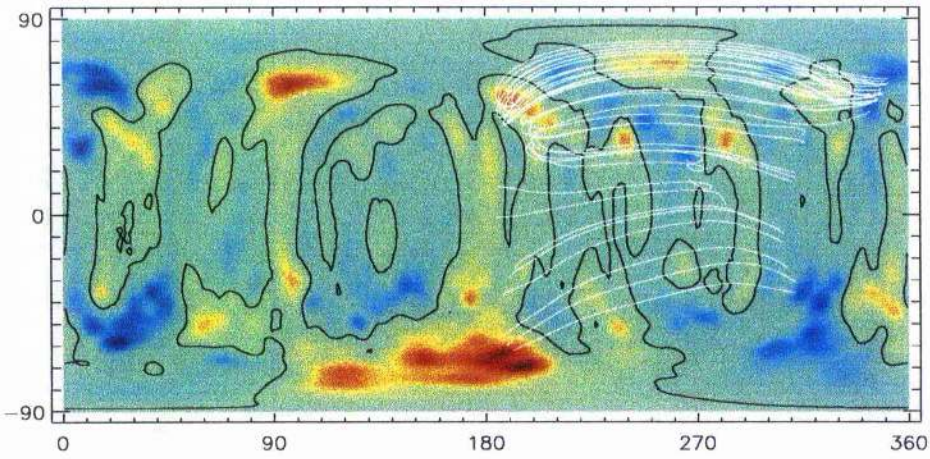


Figure 4.15: This shows the fieldlines responsible for the rest of the stable surface

Figure 4.16: This shows the rest of the stable surface and the fieldlines responsible for it

CHAPTER 5

# Adding a dipole and a source surface quasidipole

In the previous chapter, I showed that– from the observed field– it should be possible for stable points to exist at a wide variety of latitudes and distances from the star.

However, I also commented that Donati et al. (2000) had shown that for the ultra–fast rotator, RXJ1508.6–4432, prominences tend to form in the equatorial plane, near and beyond the corotation radius.

How are these to be reconciled? In chapter 3 I investigated the equlibrium surfaces for a dipole, and found that the they were confined to the equatorial plane, and were beyond $r_L$. Could there be an extra dipolar component to the field?

## 5.1 Adding a dipole

I investigated adding a dipole field $q\mathbf{B_d}$, where $q$ indicates the strength of the field, to a potential field $\mathbf{B}_p$. $q$ is $B_\theta(r_K, \pi/2, \phi)$ for a dipole field, so from equation 3.6 and the equations for a dipole field (3.10–3.12), it is related to $B_0$ by

$$q = \frac{B_0\omega^2}{GM_*} \tag{5.1}$$

Equation (3.1) becomes

$$\mathbf{g}.(\mathbf{B_p} + q\mathbf{B_d}) = 0.$$

so the value of $q$ at any particular point to satisfy this equation is given by

$$q = -\frac{\mathbf{g}.\mathbf{B_p}}{\mathbf{g}.\mathbf{B_d}}. \tag{5.2}$$

Obviously, equation 5.2 only holds when $\mathbf{g}.\mathbf{B_d} \neq 0$– the points where $\mathbf{g}.\mathbf{B_d} = 0$ are those in the equatorial plane and those where equation 3.14 holds.

This means the LHS of (3.2) becomes

$$\mathbf{B_p}.\nabla(\mathbf{g}.\mathbf{B_p}) + q[\mathbf{B_d}.\nabla(\mathbf{g}.\mathbf{B_p}) + \mathbf{B_p}.\nabla(\mathbf{g}.\mathbf{B_d})] + q^2\mathbf{B_d}.\nabla(\mathbf{g}.\mathbf{B_d}) \tag{5.3}$$

However, in the equatorial plane $\mathbf{g}.\mathbf{B_d} = 0$, so adding a dipole field doesn't change $\mathbf{g}.\mathbf{B}$. However, adding a dipole will change $\mathbf{B}.\nabla(\mathbf{g}.\mathbf{B})$. It is this which I decided to look at by adding a dipole.

(5.3) can be expressed in the form $aq^2+bq+c$ where $a = \mathbf{B_d}.\nabla(\mathbf{g}.\mathbf{B_d})$, $b = \mathbf{B_d}.\nabla(\mathbf{g}.\mathbf{B_p}) + \mathbf{B_p}.\nabla(\mathbf{g}.\mathbf{B_d})$ and $c = \mathbf{B_p}.\nabla(\mathbf{g}.\mathbf{B_p})$. Hence the values of $q$ (if any) which make (5.3) $< 0$ can be calculated using the quadratic formula.

For the 1996 night 1 and 1995 data, points in the equatorial plane where $r < r_L$ can be classified into two groups:

- ones which are unstable $\forall q$ and
- ones which are stable only for a limited range of values of $q$.

For the 1995 data, the extreme values of $q$ for stability are -24.796 and 37.534. Outside these values, there is no stability within the region under consideration. However these both occur with r=0.8665, which is nearly at the outer edge. If we consider the equatorial plane up to r=0.8 then these values of $q$ range from -8.138 to 8.855.

These can be summarised in table 5.1

The values of $q_{min}$ and $q_{max}$ as given by table 5.1 do not change as $r_{max}$ is decreased from 0.8 to 0.4. This is because these values of $q_{min}$ and $q_{max}$ correspond to points closer in to the surface. Hence, as $|q|$ is increased, then, in the equatorial plane out to $r = 0.8$ in Wilson-Devinney units, it is some points near the surface which remain stable for longest.

Is this unique to the 1995 data? For points in the equatorial plane where$r < r_L$ for the 1996 night 1 data, then the extreme values of $q$ for stability are -4.321 and 25.992, a much narrower range than for 1995. Moreover, $q_{max}$ occurs at r=0.8665, the outer edge of the region under consideration, whereas $q_{min}$ occurs at r=0.3951, the inner edge of the region.

| $r_{max}$ | $q_{min}$ | $q_{max}$ |
|---|---|---|
| $r_L$ | -24.796 | 37.534 |
| 0.8 | -8.138 | 8.855 |
| 0.7 | -8.138 | 8.855 |
| 0.5 | -8.138 | 8.855 |
| 0.4 | -8.138 | 8.855 |

Table 5.1: This table shows the extreme values of $q$ out to certain distances from the centre of the star. Between the surface and $r_{max}$ there are no stable points in the equatorial plane if $q < q_{min}$ or $q > q_{max}$. This is for the 1995 data.

| $r_{max}$ | $q_{min}$ | $q_{max}$ |
|---|---|---|
| $r_L$ | -4.321 | 25.992 |
| 0.8 | -4.321 | 3.670 |
| 0.7 | -4.321 | 3.670 |
| 0.5 | -4.321 | 3.670 |
| 0.4 | -4.321 | 3.670 |

Table 5.2: This table shows the extreme values of $q$ out to certain distances from the centre of the star. Between the surface and $r_{max}$ there are no stable points in the equatorial plane if $q < q_{min}$ or $q > q_{max}$. This is for the 1996 night 1 data.

A similar table to 5.1 for the 1996 night 1 data is 5.2.

The next step was to choose values of $q$ and plot the stable surfaces for them. The values chosen were 0 (equivalent to the potential field calculated from the observations), $\pm\frac{1}{10}$, $\pm\frac{1}{3}$, $\pm1$, $\pm3$ and $\pm10$.

For the 1996 night 1 data, figures 3.7–3.12 show that the stable surface within $r_L$ is concentrated to one side of the star, and that outside $r_L$ is concentrated into one feature (feature I), which extends from slightly above the equatorial plane to well below it.

Adding a dipole field with $q = \frac{1}{10}$, as shown in figures 5.1 and 5.2, feature I has grown smaller and is concentrated above the equatorial plane. In addition, there is a new feature (feature II) which lies $\sim180°$ in longitude from feature I and is predominantly below the equatorial plane.

Figure 5.1: The stable surface for 1996 night 1, viewed from the pole, with a dipole of $q = 1/10$ added.

Figure 5.2: The stable surface for 1996 night 1, viewed from the equator, with a dipole of $q = 1/10$ added.

Figure 5.3: The stable surface for 1996 night 1, viewed from $i = 60°$, with a dipole of $q = 0$ added.

Are features I and II related? To investigate this I compared figures 5.3 and 5.4, which show a view from an inclination of 60°.

These figures suggest that the two features could be part of the same one.

Next, adding a dipole field with $q = \frac{1}{3}$, as shown in figures 5.5 and 5.7, seems to be similar to that with $q = \frac{1}{10}$. It is when a dipole field with $q = 1$ is added that the structure changes dramatically ...

With $q = 1$ the stable surfaces are very different to those with smaller values of $q$. As figures 5.6 and 5.8 show, the structure outside of $r_L$ forms one sheet inclined to the equatorial plane, and is nearly complete, with only a small gap, and appears to be slightly oval-shaped. Inside $r_L$ most of the stable surface seen with smaller values of $q$ has been cleared, but there still is some structure within $r_L$. The stable surface being inclined is also made clear by figure 5.9.

As figures 5.10, 5.11 and 5.12 show, when $q$ is increased to 3, most of the remaining structure within $r_L$ is cleared, and the stable surface outside of $r_L$ is complete and is less inclined to the equatorial plane than was the case when $q = 1$.

Increasing $q$ to 10, as shown in figures 5.13 and 5.14 leaves the structure looking similar to that for a dipole (figures 3.1 and 3.3). This is consistent with the values of $q_{max}$ and $q_{min}$

Figure 5.4: The stable surface for 1996 night 1, viewed from $i = 60°$, with a dipole of $q = 1/10$ added.

Figure 5.5: The stable surface for 1996 night 1, viewed from the pole, with a dipole of $q = 1/3$ added.

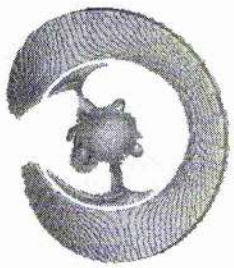

Figure 5.6: The stable surface for 1996 night 1, viewed from the pole, with a dipole of $q = 1$ added.

Figure 5.7: The stable surface for 1996 night 1, viewed from the equator, with a dipole of $q = 1/3$ added.

Figure 5.8: The stable surface for 1996 night 1, viewed from the equator, with a dipole of $q = 1$ added.

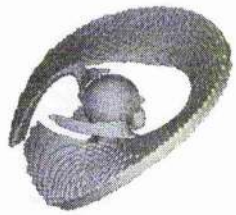

Figure 5.9: The stable surface for 1996 night 1, viewed from $i = 60°$, with a dipole of $q = 1$ added.

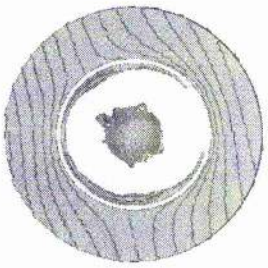

Figure 5.10: The stable surface for 1996 night 1, viewed from the pole, with a dipole of $q = 3$ added.

Figure 5.11: The stable surface for 1996 night 1, viewed from the equator, with a dipole of $q = 3$ added.

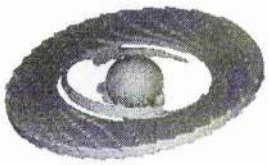

Figure 5.12: The stable surface for 1996 night 1, viewed from $i = 60°$, with a dipole of $q = 3$ added.

shown in table 5.2.

The next step is to look at adding in a dipole field with negative values of $q$. For $q = -\frac{1}{10}$ and $q = -\frac{1}{3}$, the results seem very similar to those for $q = \frac{1}{10}$ and $q = \frac{1}{3}$ respectively, as shown by figures 5.15 and 5.16 for the case where $q = -\frac{1}{10}$ and by 5.17 and 5.18 for $q = -\frac{1}{3}$.

The structure with $q = -1$, as shown in figures 5.19, 5.20 and 5.21, differs in a few ways from that with $q = 1$. The most obvious differences are that the structure with $r > r_L$ is complete (rather than having a gap in similar to that with $q = 1$) and having an opposite inclination to the equatorial plane.

With $q = -3$, as shown in figures 5.22 and 5.23, the structure is similar to that with $q = 3$, except for the structure outside of $r_L$ being inclined at opposite angles to the equatorial plane.

The final case examined for the 1996 night 1 data was for $q = -10$, shown in figures 5.24 and 5.25. As was the case for $q = 10$, the structure is similar to that for a pure dipole. By the stage $|q| = 10$, the field appears similar to that of a dipole.

When a dipole with q=±10 is added to the 1996 night 1 field, then prominences divide easily into two groups:

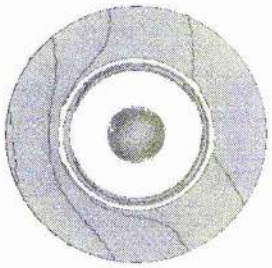

Figure 5.13: The stable surface for 1996 night 1, viewed from the pole, with a dipole of $q = 10$ added.

Figure 5.14: The stable surface for 1996 night 1, viewed from the equator, with a dipole of $q = 10$ added.

Figure 5.15: The stable surface for 1996 night 1, viewed from the pole, with a dipole of $q = -1/10$ added.

Figure 5.16: The stable surface for 1996 night 1, viewed from the equator, with a dipole of $q = -1/10$ added.

Figure 5.17: The stable surface for 1996 night 1, viewed from the pole, with a dipole of $q = -1/3$ added.

Figure 5.18: The stable surface for 1996 night 1, viewed from the equator, with a dipole of $q = -1/3$ added.

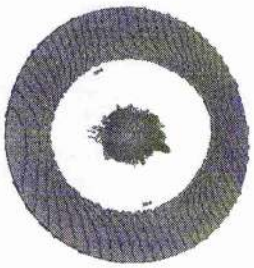

Figure 5.19: The stable surface for 1996 night 1, viewed from the pole, with a dipole of $q = -1$ added.

Figure 5.20: The stable surface for 1996 night 1, viewed from $i = 60°$, with a dipole of $q = -1$ added.

Figure 5.21: The stable surface for 1996 night 1, viewed from the equator, with a dipole of $q = -1$ added.

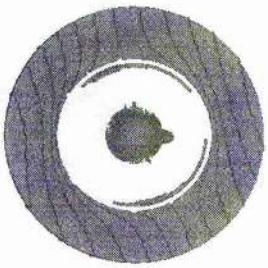

Figure 5.22: The stable surface for 1996 night 1, viewed from the pole, with a dipole of $q = -3$ added.

Figure 5.23: The stable surface for 1996 night 1, viewed from the equator, with a dipole of $q = -3$ added.

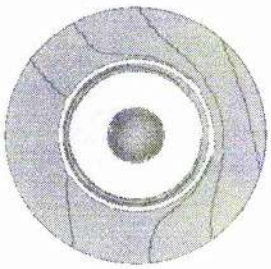

Figure 5.24: The stable surface for 1996 night 1, viewed from the pole, with a dipole of $q = -10$ added.

Figure 5.25: The stable surface for 1996 night 1, viewed from the equator, with a dipole of $q = -10$ added.

1. ones less than $0.1R_*$ from the stellar surface,
2. ones lying in the equatorial plane near and beyond the corotation radius.

## 5.2 Adding a source surface quasidipole

Although adding in a dipole ensures that the majority of stable points are in the equatorial plane and beyond $r_L$, the field obtained doesn't satisfy the source surface requirements of equation (2.4), as

$$B_r = 2\frac{B_0}{r_s^3}\cos\theta$$

and

$$B_\theta = \frac{B_0}{r_s^3}\sin\theta.$$

Hence, I decided to add in a source surface quasidipole, which has components given by equations (3.21–3.23).

As was the case for the dipole $q = B_\theta(r_K, \pi/2, \phi)$, hence

$$q = B_0\frac{(\frac{r_s}{r_K})^3 - 1}{r_K(1 + 2(\frac{r_s}{R_*})^3)}, \tag{5.4}$$

which, when using the definition of $r_K$ given by equation (3.6), gives

$$q = B_0 \frac{r_s(\frac{\omega^2}{GM_*})^{\frac{2}{3}} - (\frac{GM_*}{\omega^2})^{\frac{1}{3}}}{1 + 2(\frac{r_s}{R_*})^3}. \tag{5.5}$$

To ensure that I could compare the effects of adding a source surface quasidipole and a genuine dipole, I needed to ensure that the field strength added at the surface was equal. If $q_p$ and $q_d$ are the values of $q$ calculated by 5.5 and 5.1 respectively, then

$$q_p = \frac{2(r_s^3 - 1)}{R_*^3(1 + 2(\frac{r_s}{R_*})^3)} q_d. \tag{5.6}$$

All distances are in Wilson-Devinney units and hence are dimensionless. In these units $r_s = 2.000$ and $R_* = 0.386$ to 3 decimal places. This gives

$$q_p = 0.872 q_d. \tag{5.7}$$

A surprising result was that a small value of $q$ needed to clear out much of the disc inside $r_L$ (where $r_L$ is given by equation 3.20). Table 5.3 shows the number of stable points within $r_L$. The grid used was divided into 513 pixels in longitude, 257 in latitude and 135 radial shells. Inside $r_L$ there were 12985056 points in total.

| $q$ | number of stable points |
|---|---|
| 0 | 75354 |
| 0.05 | 34687 |
| 0.1 | 31932 |
| 0.2 | 18967 |
| 0.3 | 10196 |
| 0.4 | 4868 |
| 0.5 | 3340 |

Table 5.3: This table shows the number of stable points inside $r_L$ when a quasidipole determined by the value of $q$ is added.

A value of $q$ of only 0.05 (corresponding to the added flux at the poles being 17.3G), is sufficient to halve the number of stable points compared to the situation when there is no field added in.

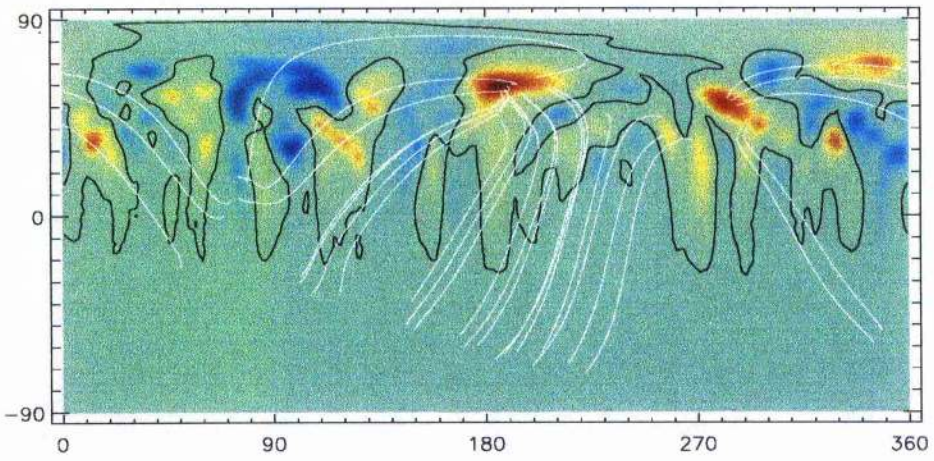


Figure 5.26: This shows the fieldlines causing the stable surface beyond $r_L$ for the 1996 night 1 field with a quasidipole ($q = 0.05$) added

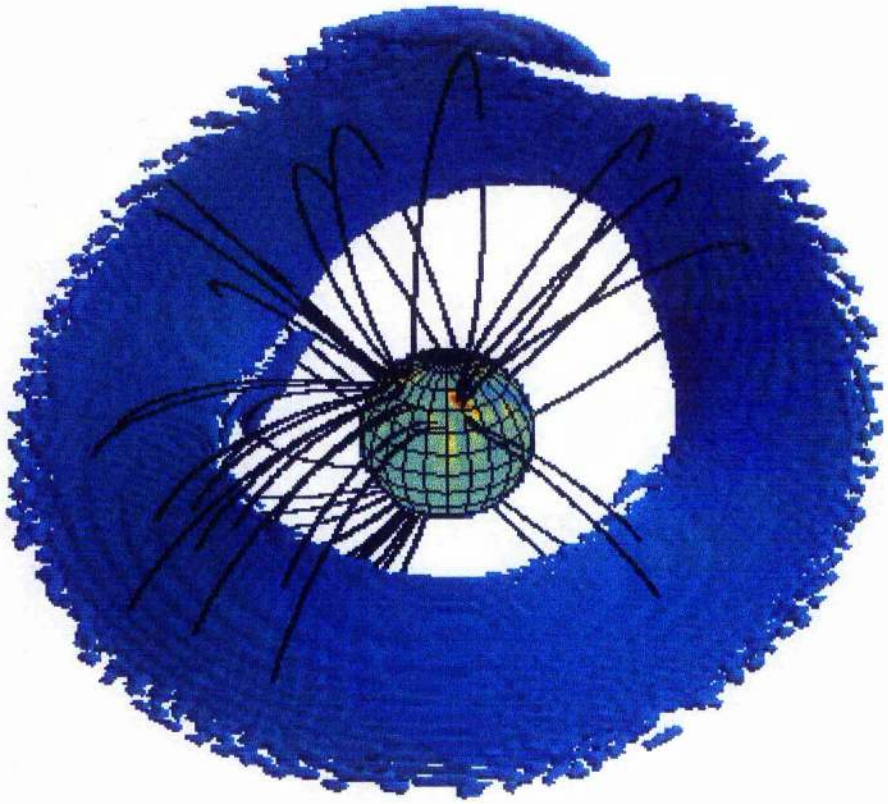

Figure 5.27: This shows the stable surface beyond $r_L$ for the 1996 night 1 field with a quasidipole ($q = 0.05$) added

CHAPTER 6

# Summary and Conclusion

## 6.1 The surface magnetic field

For the surface magnetic field, the distribution of $\alpha$ (defined by equation 2.1) is symmetric and centred on zero, implying that when new flux is created, there is no preference for the sign of $\alpha$. When the field is evolved according to diffusion and the observed differential rotation, the peak of $\alpha$ gradually moves to positive values and grows weaker, showing that diffusion and differential rotation alone are insufficient to explain the evolution of the field on timescales of about a month– but our model does not include flux emergence.

I have shown that the differential rotation can create a band of unipolar azimuthal field at high–latitudes, though of a weaker strength than that which is observed. However, differential rotation could play a part in preserving the band on unipolar azimuthal field.

## 6.2 Prominences

Using the criteria

$$\mathbf{g}.\mathbf{B} = 0$$

and

$$\mathbf{B}.\nabla(\mathbf{g}.\mathbf{B}) < 0$$

it is possible to determine where prominences can be stable. A potential field extrapolated from the observed radial field gives complex equilibrium surface structures– however Donati et al.

(2000) showed that the prominences preferentially formed at and beyond corotation and in the equatorial plane.

The possibility that this discrepancy is simply due to the unobservability of southern latitudes (which are assumed to have $\mathbf{B} \sim \mathbf{0}$ can be discounted since when a southern hemisphere field of similar complexity to the observed northern hemisphere field is added in, the equilibrium surfaces remain complex.

I have shown that adding in a source surface quasidipole of less than 20G is sufficient to clear the inner disc of stable points, and ensures that most of the stable points are at low latitudes. As Donati & Collier Cameron (1997) showed, even fields of several kG at the pole would be hard to detect– so it would be much harder to detect an added field of 20G.

# REFERENCES


Adams W. S., 1909, ApJ, 29, 110

Anders G., 1990, Inf. Bull. Variable Stars, 3437

Antiochos S. K., Klimchuk J. A., 1991, ApJ, 378, 372

Anzer U., 1969, Solar Phys., 8, 37

Ayres T. R., Linsky J. L., 1980, ApJ, 241, 279

Babcock H. W., Babcock H. D., 1955, ApJ, 121, 349

Babcock H. W., 1947, ApJ, 105, 105

Baliunas S. L., Vaughan A. H., 1985, ARA&A, 23, 379

Baliunas S. L. et al., 1985, ApJ, 294, 310

Barnes J. R., Collier Cameron A., Unruh Y. C., Donati J.-F., Hussain G. A. J., 1998, MNRAS, 299, 904

Barocas V., 1939, ApJ, 89, 486

Barrado y Navascués D., Stauffer J. R., Randich S., 1998, ApJ, 506, 347

Berger T. E., Löfdahl M. G., Shine R. A., Title A. M., 1998, ApJ, 506, 439

Bidelman W. P., MacConnell D. J., 1973, AJ, 78, 687

Boesgaard A. M., 1989, ApJ, 336, 798

Brandenburg A., Saar S. H., Turpin C. R., 1998, ApJ, 498, 151

Busso M., Scaltriti F., Cellino A., 1985, A&A, 148, 29

Byrne P. B., Eibe M. T., van den Oord G. H. J., 1998, in ASP Conf. Ser. 150: New Perspectives on Solar Prominences. ASP Conference Series, San Francisco, p. 227

Campbell W. W., 1899, ApJ, 9, 31

Carrington R. C., 1858, MNRAS, 19, 1

Carrington R. C., 1859, MNRAS, 19, 81

Clerke A. M., 1899, Observatory, 22, 152

Collier Cameron A., Foing B. H., 1997, Observatory, 117, 218

Collier Cameron A., Robinson R. D., 1989a, MNRAS, 236, 57

Collier Cameron A., Robinson R. D., 1989b, MNRAS, 238, 657

Collier Cameron A., Unruh Y. C., 1994, MNRAS, 269, 814

Collier Cameron A., Woods J. A., 1992, MNRAS, 258, 360

Collier Cameron A., Bedford D. K., Rucinski S. M., Vilhu O., White N. E., 1988, MNRAS, 231, 131

Collier Cameron A., Duncan D. K., Ehrenfreund P., Foing B. H., Kuntz K. D., Penston M. V., Robinson R. D., Soderblom D. R., 1990, MNRAS, 247, 415

Collier Cameron A., 1988, MNRAS, 233, 235

Collier Cameron A., 1995, MNRAS, 275, 534

Collier Cameron A., 1999, in ASP Conf. Ser. 158: Solar and Stellar Activity: Similarities a nd

Differences. ASP Conference Series, San Francisco, p. 146

Council of the Royal Astronomical Society, 1852, MNRAS, 12, 105

Dahlburg R. B., Antiochos S. K., Klimchuk J. A., 1998, ApJ, 495, 485

Donahue R. A., Saar S. H., Baliunas S. L., 1996, ApJ, 466, 384

Donati J.-F., Brown S. F., 1997, A&A, 326, 1135

Donati J.-F., Collier Cameron A., 1997, MNRAS, 291, 1

Donati J.-F., Collier Cameron A., Hussain G. A. J., Semel M., 1999, MNRAS, 302, 437

Donati J.-F., Mengel M., Carter B. D., Marsden S., Collier Cameron A., Wichmann R., 2000, MNRAS, 316, 699

Duncan D. K. et al., 1991, ApJS, 76, 383

Duncan D. K., 1981, ApJ, 248, 651

Eberhard G., Schwarzschild K., 1913, ApJ, 38, 292

Ferreira J. M., 2000, MNRAS, In press

Frazier E. N., 1970, Solar Phys., 14, 89

Friel E. D., Boesgaard A. M., 1992, ApJ, 387, 170

Giampapa M. S., 1984, ApJ, 277, 235

Gray D. F., 1984, ApJ, 277, 640

Greenstein J. L., Richardson R. S., 1951, ApJ, 113, 536

Güdel M. et al., 2001, A&A, 365, L336

Hale G. E., Ellerman F., Nicholson S. B., Joy A. H., 1919, ApJ, 49, 153

Hale G. E., 1908a, PASP, 20, 220

Hale G. E., 1908b, PASP, 20, 287

Hale G. E., 1908c, ApJ, 28, 100

Hale G. E., 1908d, ApJ, 28, 315

Herbig G. M., 1965, ApJ, 141, 588

Herbig G. H., 1985, ApJ, 289, 269

Hirshfield A., Sinnott R. W., 1982, Sky Catalogue 2000.0 Vol.1: Stars to magnitude 8.0. Sky Publishing Corporation and Cambridge University Press

Howard R., 1959, ApJ, 130, 193

Huggins W., Huggins M. L., 1897, ApJ, 6, 77

Innis J. L., Robinson R. D., Coates D. W., Thompson K., 1985, Proc. Astron. Soc. Aust., 6, 156

Innis J. L., Thompson K., Coates D. W., Lloyd Evans T., 1988, MNRAS, 235, 1411

Innis J. L., Thompson K., Coates D. W., 1986, MNRAS, 223, 183

James D. J., Jardine M., Jeffries R. D., Randich S., Collier Cameron A., Ferreira J. M., 2000, MNRAS, In press

Jardine M., Ferreira J. M. T. S., 1996, Astrophysical Letters and Communications, 34, 10

Jardine M., Unruh Y. C., 1999, A&A, 346, 883

Jardine M., Barnes J. R., Unruh Y., Collier Cameron A., 1998, in ASP Conf. Ser. 150: New Perspectives on Solar Prominences. ASP Conference Series, San Francisco, p. 235

Jardine M., Barnes J., Donati J.-F., Collier Cameron A., 1999, MNRAS, 305, L35

Kippenhahn R., Schlüter A., 1957, Z. Astrophys., 43, 36

Kitchatinov L., Rüdiger G., 1999, A&A, 344, 911

Kürster M., Schmitt J. H. M. M., Cutispoto G., Dennerl K., 1997, A&A, 320, 831

Kürster M., Schmitt J. H. M. M., Cutispoto G., 1994, A&A, 289, 899

Lebreton Y., Gomez A. E., Mermilliod J.-C., Perryman M. A. C., 1997, ESA Symp. 402: Hipparcos - Venice '97, 402, 231

Leighton R. B., 1959, ApJ, 130, 366

Li J., Collier Cameron A., 1993, MNRAS, 261, 766

Lim J., Nelson G. J., Castro C., Kilkenney D., van Wyk F., 1992, ApJ, 388, L27

Lim J., White S. M., Nelson G. J., Benz A. O., 1994, ApJ, 430, 332

Lockyer N., Lockyer W. J. S., 1903, MNRAS, 63, A6

Lockyer W. J. S., 1903, MNRAS, 63, 423

Maggio A., Sciortino S., Vaiana G. S., Majer P., Bookbinder J., Golub L., Harnden F. R., Rosner R., 1987, ApJ, 315, 687

Maggio A., Pallavicini R., Reale F., Tagliaferri G., 2000, A&A, 356, 627

Marcy G. W., 1982, PASP, 94, 989

Maunder E. W., 1913, MNRAS, 74, 112

Mermilliod J. C., 1981, ApJ, 97, 235

Mewe R., Kaastra J. S., White S. M., Pallavicini R., 1996, A&A, 315, 170

Micela G., Sciortino S., Vaiana G. S., Bookbinder J., Golub L., Rosner R., 1985, ApJ, 292, 172

Micela G., Sciortino S., Vaiana G. S., Schmitt J. H. M. M., Stern R. A., Harnden F. R., Rosner R., 1988, ApJ, 325, 798

Minnaert M., 1937, Observatory, 60, 292

Mullan D. J., 1979, ApJ, 231, 152

Mutschlecner J. P., 1963, AJ, 68, 287

Nicholson S. B., Sternberg E. E., 1934, PASP, 46, 225

Noyes R. W., Hartmann L., Baliunas S. L., Duncan D. K., Vaughan A. H., 1984, ApJ, 279, 763

Noyes R. W., Weiss N. O., Vaughan A. H., 1984, ApJ, 287, 769

Pakull M. W., 1981, A&A, 104, 33

Pallavicini R., Golub L., Rosner R., Vaiana G. S., Ayres T., Linsky J. L., 1981, ApJ, 248, 279

Pettit E., 1939, PASP, 51, 289

Pettit E., 1943, PASP, 55, 184

Pikel'ner S. A., 1971, Solar Phys., 17, 44

Poland A. I., Mariska J. T., 1986, Solar Phys., 104, 303

Preston G. W., 1971, ApJ, 164, 309

Priest E. R., Smith E. A., 1979, Solar Phys., 64, 267

Priest E. R., Hood A. W., Anzer U., 1989, ApJ, 344, 1010

Priest E. R., 1984, Solar Magnetohydrodynamics. D. Reidel, Dordrecht

Prosser C. F., Randich S., Stauffer J. R., Schmitt J. H. M. M., Simon T., 1996, AJ, 112, 1570

Randich S., Schmitt J. H. M. M., 1995, A&A, 298, 115

Randich S., Schmitt J. H. M. M., Prosser C. F., Stauffer J. R., 1995, A&A, 300, 134

Randich S., Schmitt J. H. M. M., Prosser C. F., 1996, A&A, 313, 815

Raynard A. C., 1879, Mem. R. Astron. Soc., 41

Roberts W. O., 1948, ApJ, 108, 523

Robichon N., Arenou F., Turon C., Mermilliod J.-C., Lebreton Y., 1997, ESA Symp. 402: Hipparcos - Venice '97, 402, 567

Robinson R. D., Collier Cameron A., 1986, Proc. Astron. Soc. Aust., 6, 308

Robinson R. D., Worden S. P., Harvey J. W., 1980, ApJ, 236, L155

Robinson R. D., 1980, ApJ, 239, 961

Rucinski S. M., 1982, Inf. Bull. Variable Stars, 2203

Rush J. H., Trotter D. E., 1954, AJ, 59, 191

Saar S. H., Brandenburg A., 1999, ApJ, 524, 295

Schatten K., Wilcox J., Ness N., 1969, Solar Phys., 6, 442

Schmitt J. H. M. M., Cutispoto G., Krautter J., 1998, ApJ, 500, L25

Schmitt J. H. M. M., Golub L., Harnden F. R., Maxson C. W., Rosner R., Vaiana G. S., 1985, ApJ, 290, 307

Schmitt J. H. M. M., Micela G., Sciortino S., Vaiana G. S., Harnden F. R., Rosner R., 1990, ApJ, 351, 492

Schrijver C. J., Coté J., Zwann C., Saar S. H., 1989, ApJ, 337, 964

Schrijver C. J., 1983, A&A, 127, 289

Schrijver C. J., 1987, A&A, 172, 111

Schrijver C. J., 1991, in Reviews of Modern Astronomy. p. 18

Sheeley N. R., 1967, ApJ, 147, 1106

Shima M., Honda M., 1963, J. Geophys. Res., 68, 2849

Skumanich A., Smythe C., Frazier E. N., 1975, ApJ, 200, 747

Skumanich A., 1972, ApJ, 171, 565

Slee O. B., Nelson G. J., Innis J. L., Stewart R. T., Vaughan A., Wright A. E., 1986, Proc. Astron. Soc. Aust., 6, 312

Soderblom D. R., Stauffer J. R., MacGregor K. B., Jones B. F., 1993, ApJ, 409, 624

Stauffer J. R., Hartmann L. W., Prosser C. F., Randich S., Balachandran S., Patten B. M., Simon T., Giampapa M., 1997, ApJ, 479, 776

Stępień K., 1989, Acta Astron., 210, 273

Stimets R. W., Giles R. H., 1980, ApJ, 242, L37

Unruh Y. C., Collier Cameron A., Cutispoto G., 1995, MNRAS, 277, 1145

van Ballegooijen A., Cartledge N., Priest E., 1998, ApJ, 501, 866

Vaughan A. H., Preston G. W., 1980, PASP, 92, 385

Vaughan A. M., Preston G. W., Wilson O. C., 1978, PASP, 90, 267

Vaughan A. H., Baliunas S. L., Middelkoop F., Hartmann L., Mihalas D., Noyes R. W., Preston G. W., 1981, ApJ, 250, 276

Vaughan A. H., 1980, PASP, 92, 392

Vilhu O., Gustafsson B., Edvardsson B., 1987, ApJ, 320, 850

Vilhu O., Tsuru T., Collier Cameron A., Budding E., Banks T., Slee B., Ehrenfreund P., Foing B. H., 1993, A&A, 278, 467

Vilhu O., 1984, A&A, 133, 117

Vogt S. S., Penrod G. D., 1983, PASP, 95, 565

Wallerstein G., Herbig G. H., Conti P. S., 1965, ApJ, 141, 610

Walter F. M., 1981, ApJ, 245, 677

Walter F. M., 1982, ApJ, 253, 745

Walter F. M., 1983, ApJ, 274, 794

Walter F. M., 1999, in ASP Conf. Ser. 158: Solar and Stellar Activity: Similarities and Differences. ASP Conference Series, San Francisco, p. 87

Weber E. J., Davis L., 1967, ApJ, 148, 217

White O. R., Livingston W. C., 1981, ApJ, 249, 798

Wilson O. C., Bappu M. K. V., 1957, ApJ, 125, 661

Wilson O. C., Skumanich A., 1964, ApJ, 140, 1401

Wilson O. C., 1959, ApJ, 130, 499

Wilson O. C., 1963, ApJ, 138, 832

Wilson O. C., 1966, ApJ, 144, 695

Wilson O. C., 1968, ApJ, 153, 221

Wilson O. C., 1978, ApJ, 226, 379

Wittmann A. D., Xu Z. T., 1987, A&AS, 70, 83

Wolff S. C., Boesgaard A. M., Simon T., 1986, ApJ, 310, 360

Wolk S. J., Walter F. M., 1996, AJ, 111, 2066

Wright W. H., 1910, Lick. Obs. Bull., 6, 60

Zirin H., 1988, Astrophysics of the Sun. Cambridge University Press, Cambridge and New York